

INVESTIGATION OF THE RESPONSE OF NIMH CELLS TO BURP CHARGING

A Dissertation

Presented to

the Faculty of the Department of Chemical Engineering

University of Houston

In Partial Fulfillment of the Degree

Doctor of Philosophy

in Chemical Engineering

by

Eric C. Darcy

December 1998

INVESTIGATION OF THE RESPONSE OF NIMH CELLS TO BURP CHARGING

Eric C. Darcy

Approved:

Chairman of the Committee
Kishore Mohanty, Professor
Chemical Engineering

Committee Members:

Demetre J. Economou, Professor
Chemical Engineering

Richard Willson, Professor
Chemical Engineering

Allan J. Jacobson, Professor,
Chemistry

Scott S. Perry, Assistant Professor,
Chemistry

Richard Pollard, Scientist and Technical Leader,
The Dow Chemical Company

Charles Dalton, Associate Dean,
Cullen College of Engineering

James T. Richardson, Professor and Chairman,
Chemical Engineering

ACKNOWLEDGEMENTS

The advice and support of a number teachers, supervisors, colleagues, friends, and family made this work possible for which I wish to express enormous gratitude.

Dr. R. Pollard's guidance, insightful advice, and unwavering support as my research advisor has been invaluable. Dr. K. Mohanty also deserves thanks for volunteering to be my advisor at the end in place of Dr. Pollard. Also instrumental are my supervisors during the work, T. Davies, B. Wittschen, and W. Brasher. They made possible the resources to work on this endeavor and had the necessary patience while some of my "real" NASA work was delayed.

Bill Tipton provided me with what seem to be an endless supply of KOH solutions along very useful laboratory experimental advice. Glenn Morgan's assistance during the SEM and EDS work deserves recognition. The detailed electrical design of the battery cyclers would not have been possible without S. Hossain and B. Hughes must be commended for his persistence to keep it free of hardware bugs.

I want thank my co-workers, B. Bragg, E. Kluksdahl, D. Allison, and S. Lazaroff for their encouragement and for stepping-in to take on some of my NASA always growing projects, which allowed me to dedicate more time to this work. Also deserving thanks are my mountain climbing buddies D. Schneider, D. Young, and T. Barrera, who along with my Dad, provided the necessary nagging reminders that I needed to stay on course, by perpetually asking me, "How is that thesis going? Any progress?"

The final compilation of this work would not have been possible without the selfless help of my in-laws, Paul and Rosetta. They are fantastic grand-parents, particularly to our 2 year old daughter, and they stood in for me while I was away for many nights and week-ends compiling this dissertation.

Finally, I must thank my wife, Cheryl, for her incredible patience, tremendous love, and her understanding support through some difficult times along the journey of this work. A better friend, I could not have.

INVESTIGATION OF THE RESPONSE OF NIMH CELLS TO BURP CHARGING

An Abstract

of a

Dissertation

Presented to

the Faculty of the Department of Chemical Engineering

University of Houston

In Partial Fulfillment of the Degree

Doctor of Philosophy

in Chemical Engineering

by

Eric C. Darcy

December 1998

An Abstract

of a

Dissertation

Performance cycling and calorimetric analysis of nickel metal hydride cells have revealed that reverse pulse (“burp”) charging improves performance over other charging techniques. Burp charging periodically applies a short-duration, high-rate discharge pulse followed by a short rest during an otherwise galvanostatic charge. Results show improved charge input and output, lower heat generation during charge, lower charge overvoltage, and no loss of cycle life. Several hypotheses for the responsible phenomena were examined. In-situ video-microscopic analysis of the cell and its nickel electrode during charge revealed the significance of the gas evolution reactions. In-situ gas generation rate measurements made manometrically during charge determined that the burp pulse sequence results in less gas generation than galvanostatic charging. Evidence is presented that the “burp” pulse sequence electrochemically consumes gas bubbles generated during charge at the positive and negative electrodes, respectively. Removing bubbles increases the effective electrode surface area, results in a lower charge overvoltage, and reduces cell pressure.

TABLE OF CONTENTS

1.0 Introduction (Chapter 1)	
1.1 Statement of the Problem.....	11
1.2 Motivation.....	11
1.3 Background and Review of Previous Work.....	13
2.0 Description of Experiment (Chapter 2)	
2.1 Performance Cycling.....	18
2.2 Cell Calorimetry.....	19
2.3 Destructive Physical Analysis.....	19
2.4 Video-Microscopy.....	20
2.5 Manometry.....	21
3.0 Results and Discussion (Chapter 3)	
3.1 Performance Cycling.....	23
3.2 Cell Calorimetry.....	25
3.3 Destructive Physical Analysis.....	27
3.4 Video-Microscopy.....	30
3.5 Manometry.....	31
3.6 Summary and Conclusions (Chapter 4).....	43
3.7 References.....	45
6.0 Appendices	
A. Design, Specifications, and Operation of Battery Cycling Experiment.....	47
B. Design, Specifications and Operation of Cell Calorimetry Experiment.....	59
C. Set-up and Procedure for Destructive Physical Analysis.....	61
D. Set-up and Procedure for Video-Microscopy.....	63
E. Set-up and Procedure for Manometry.....	65

LIST OF FIGURES

Fig. 1.	Typical reverse pulse (burp) current waveform.	13
Fig. 2.	Simple galvanostatic charging effects on cycle life.	23
Fig. 3.	Smart versus simple galvanostatic charging. Comparison of discharge output versus cycle life.	24
Fig. 4.	Burp charging versus smart galvanostatic charging. Comparison of discharge output versus cycle life.	25
Fig. 5.	Calorimetric comparison of galvanostatic and pause charging. Charge heat and voltage comparison versus time.	26
Fig. 6.	Calorimetric comparison of the three charge waveforms. Charge heat and overvoltage versus time.	27
Fig. 7.	Comparison of the charge overvoltage and gas generation of three charge methods (burp, pause, and galvano) versus runtime with the same nickel metal hydride cell. Initiation of 2 nd charge/discharge cycle for each method was at a runtime of 0 minutes. Gas generation volume indicated by centimeters of water displaced in a manometer. Current levels; Burp at 2.000A, Pause at 1.974A, Galvano at 1.915A.	32
Fig. 8.	Comparison of the end of charge with exaggerated pause and burp waveforms versus runtime with the same nickel metal hydride cell. Initiation of the charge was at a runtime of 0 minutes.	35
Fig. 9.	Voltage and gas evolution curves versus runtime during a charge rest period followed by cell discharge into a 0.5 ohm load.	36
Fig. 10.	Comparison of voltage and gas levels in a flooded and nominal cell during galvanostatic charge at 1.915A, rest, and resistive discharge at 0.5 ohm.	39
Fig. 11.	Cell gas and voltage level during charging of a flooded NiMH cell. Comparison of galvanostatic, pause, and burp charge methods.	41
Fig. A1.	Automated 10 Station Battery Cycler with adjacent calorimeter. Power supplies are adjacent to Charger Assembly Racks. Batteries are positioned in 3 layer holder placed on top of calorimeter.	49
Fig. A2.	Close-up of a charger assembly rack partially retreated from its slot to show its charger controller IC on printer circuit board in front of small fan.	52
Fig. B1.	Cross section of cell calorimetry experiment.	60
Fig. D1.	Schematic of the in-situ video-microscopic experiment. Charge/discharge cycler and electrical connections not shown for clarity.	64
Fig. E1.	Configuration of nominal cell with manometer. Glass spheres taking up extra volume in cylinder containing cell are not shown for clarity. Cell had small hole drilled into its negative end.	66

LIST OF FIGURES (Cont.)

Fig. E2. Configuration of flooded cell with manometer. Cell had small holes drilled into its negative and positive ends. 67

LIST OF TABLES

1. Description of waveforms compared during video-microscopic experiments.	21
2. Nickel electrode surface area and pore volume comparison.	29
3. Comparison particle size distribution of metal hydride electrodes with each charge technique.	29

NOMENCLATURE

Burp	Industrial jargon for a short-duration, high-rate discharge pulse during charge
C-rate	The discharge or charge current, in amperes, expressed as multiple of the rated capacity in ampere-hours
DOD	Depth-of-discharge
DPA	Destructive Physical Analysis
EDS	Energy Dispersion Spectroscopy
GPIB	General Purpose Instrument Bus
IC	Integrated circuit
JSC	Johnson Space Center
LED	Light emitting diode
NASA	National Aeronautics and Space Administration
NiMH	Nickel metal hydride
NiCd	Nickel cadmium
N:P	Negative to positive electrode active mass ratio
OCV	Open circuit voltage
RAM	Random access memory
SEM	Scanning Electron Microscopy
SOC	State-of-charge
TLD	Talker Listener Device
VI	Virtual Instrument, LabVIEW® subroutine

CHAPTER 1: INTRODUCTION

1.1 Statement of the Problem

Over the last 20 or more years, numerous alternatives to galvanostatic (constant current) battery charging have been tried in a more or less trial and error approach to minimize charge time and/or maximize battery discharge performance of rechargeable batteries without sacrificing their cycle life. One particular periodic method, called “burp” charging, uses a very short reverse (discharge) pulse followed by a short pause in an otherwise galvanostatic charge regime [1]. This method, also called reflex charge, has been reported to improve the performance and life of commercial nickel cadmium (NiCd) batteries [2, 3]. In addition, results of my cycling tests demonstrate the improved performance and cycle life of sealed commercial nickel metal hydride (NiMH) batteries when using burp charging. These results are detailed in Chapter 3 herein.

The problem is that, to my knowledge, there is no clear, supported explanation of the phenomena responsible for how and why cells (particularly, sealed NiMH cells) benefit from this alternative waveform.

1.2 Motivation

The proliferation of consumer, industrial, military, and aerospace applications for rechargeable batteries have resulted in a world wide battery industry with annual sales exceeding \$20 billion and growing every year at a rapid rate thanks to advances in consumer electronics, lower power requirements, and the increasing demand for portable electronic products [4]. Future battery sales will escalate by many factors if and when electric vehicles become a more prominent alternative to current internal combustion vehicles.

The great majority of NiCd, NiH₂, and NiMH cells are designed with the positive nickel electrode being active material limited because excess negative electrode active material is needed to recombine the inevitable oxygen gas produced during charging and overcharging. Typical N:P (negative to positive active material) ratios range from 1.25 to 1.95 for typical NiCd and NiMH cell designs [5, 6]. Keeping the cell gas pressure within levels that do not require thick cell casing and/or relief valve operation is critical. If excess pressure is vented, water and/or reactants are lost. This alters the relative states of the charge of the electrodes, leads to higher internal resistance, and eventually degrades cycle life. The amount of excess

negative electrode active material designed into a cell is related to the expected rates of oxygen generation at the nickel electrode during charging. The negative hydride electrode mass makes up about 50% of typical current commercial cell designs [5]. Thus, any charge method which reliably reduces that oxygen generation rate allows a reduction in the N:P ratio and make feasible higher capacity and higher energy density cell designs.

Consequently, any charge method which improves battery performance and life can have a very significant impact on current and future battery designs. This is particularly true with aerospace battery applications where batteries with higher gravimetric and volumetric energy densities and longer cycle life are always aggressively sought.

Furthermore, today's commercial burp chargers, available in an integrated circuit, apply the current waveform consistently at about 1 Hz throughout the charge sequence. A typical burp charge current waveform is shown in Figure 1. The 5 millisecond discharge pulse current level is typically set at -2.5 times the charge current level. Including its 29 millisecond current pause, one cost of the burp waveform is that it effectively charges at a rate 5% slower than a galvanostatic waveform set at the same charge current. Understanding the phenomena responsible for the benefits of this sequence will guide improvements. For example, would a variable frequency burp charging waveform which increases frequency with increasing state of charge (hence, with increasing oxygen gas generation rate) be more effective? What role does the 24 millisecond pause after the "burp" play in producing the observed effect? Which is more beneficial, the pause or the burp?

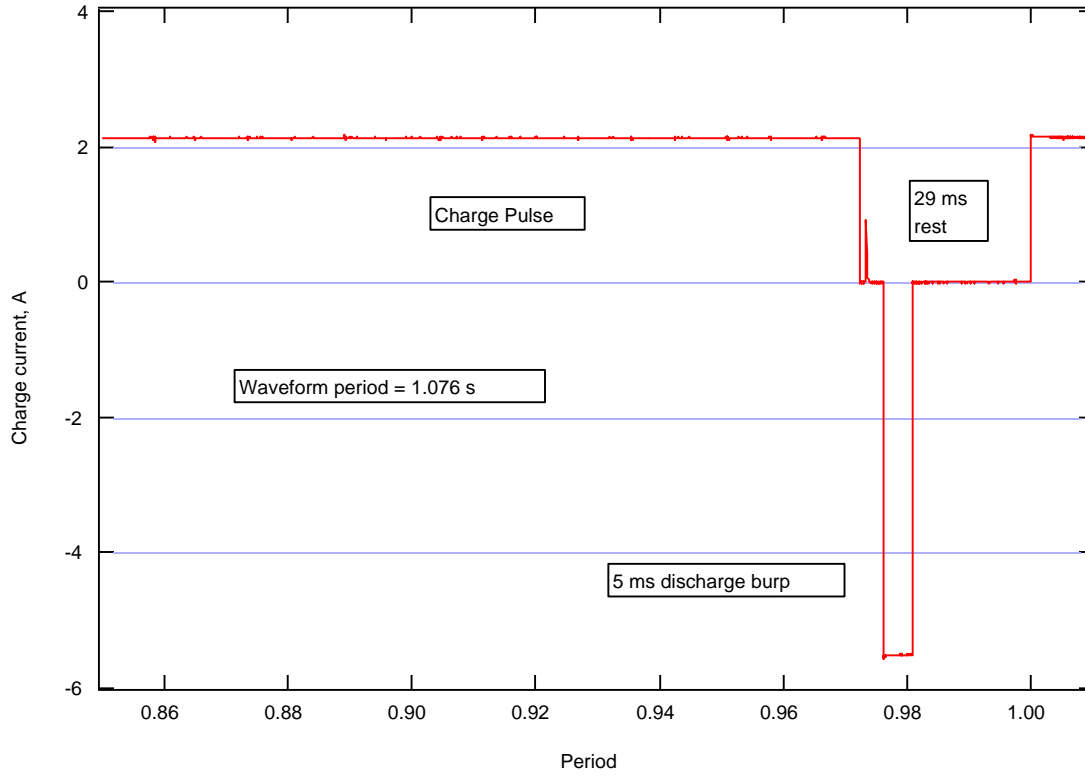


Fig. 1. Typical reverse pulse (burp) current waveform.

1.3 Review of Previous Work

With the Ni-Cd, Ni-H₂, and Ni-MH cells, at the positive electrode, nickel hydroxide (Ni(OH)₂) is the discharged active material and is oxidized to nickel oxyhydroxide (NiOOH) to become the charged active material during charge by the following electrochemical half-reaction;



Competing with this reaction, is the undesirable oxygen gas evolution half-reaction,



The degree of absence of reaction 2 largely determines the charge efficiency. It is generally observed that charge efficiency increases with decreasing temperature and vice-versa. This is because the oxygen evolution potential varies more with temperature than does the potential for reaction 1 [7]. Cell manufacturers put additives such as lithium and cadmium in the nickel electrode to raise this oxygen overpotential or reduce the nickel oxidation potential to obtain decent charge efficiency at higher temperatures [8]. Generally, at the beginning of charge, reaction 1 is highly preferred over reaction 2, but, as the state of charge increases with the charge overpotential applied, the oxygen evolution reaction becomes more significant. If charging is continued after nearly all the nickel hydroxide has been oxidized, then reaction 2 will be a prominent overcharge reaction and large amount of bubbling can be expected at the electrode surface.

For the NiMH cell, the electrochemical half-reaction on the metal hydride electrode during charge is



As mentioned before, sealed-cell designers typically put in more negative active material (MH) than positive active material to keep hydrogen pressures lower and help recombine the oxygen gas generated during overcharge by the following chemical reaction [4, 9],



This requires oxygen gas transport from the positive electrode, through the separator, and to the negative electrode. The combination of reactions 2, 3, and 4 results (at least on paper) in no electrochemical or chemical change in the cell. Ideally, reaction 4 is sufficiently facile to prevent the build up of oxygen gas and prevent the negative hydride electrode from being fully charged which would result in the build up of hydrogen gas via,



which generates hydrogen gas by water electrolysis during charge. However, if reaction 2 produces oxygen gas at a faster rate than reaction 4 can consume it, then cell pressure builds up. This can lead to cell venting, leading to permanent cell failure.

Reaction 5 is an undesirable electrochemical alternative to reaction 3. It was recently determined that reaction 5 is not only a significant overcharge reaction but can be prevalent during charging at high rates due to diffusion limitations of adsorbed atomic hydrogen into the bulk of certain metal hydrides [10] via the following mechanism;



In other words, if reaction 7 is not fast enough to prevent accumulation of the necessary adsorbed atomic hydrogen on the metal hydride surface, these atomic hydrogens will prefer to form hydrogen gas to achieve reaction 5 via the reaction 6 followed by reaction 8 [11, 12, 13, 14];

In summary, the goal of any good charger is to maximize the charge acceptance of a battery while minimizing the heat and pressure build up in cells. In other words, minimize reaction 2 and 5 by monitoring cell parameters for the proper indication of the onset of overcharge. Unfortunately, cell pressure is not a parameter that can be practically monitored in cost conscious batteries. Furthermore, in multiple cell batteries monitoring the pressure of only one cell is risky due to inevitable cell-to-cell temperature variations, and alternatively monitoring that of all cells is inherently complex.

Since their inception, a large majority of commercial NiCd and NiMH batteries have been and are charged galvanostatically. The only differences in the various galvanostatic charge methods lie with the termination algorithm used. Voltage, voltage slope, temperature, and temperature slope termination algorithms are the most common algorithms in commercial chargers today [15].

Many charge waveforms and termination algorithms have been and are still being tried today in the pursuit of the optimum charge method. The burp charge waveform was first patented in the late 1960s [2], licensed in 1990 into a commercial integrated circuit, P/N ICS1700, and later redesigned with a soft start condition and improved termination algorithms to become the ICS1702 [16]. It has achieved commercial success and is a preferred method for NASA's space battery applications using commercial NiCd and NiMH cells, without an accepted understanding of the phenomena involved. To date, several possible explanations have been offered to explain why burp charging improves NiCd and NiMH battery performance over other charge techniques. None to date has been offered with what I consider convincing evidence.

Nevertheless, here are three such hypotheses;

- 1) Burp charging prevent/retards porosity and granular morphology changes in the porous electrodes with continual cycling. The reverse pulses prevent formation of large crystals of charged active material [3]. Larger crystals cause porosity to increase or decrease. Greater porosity can cause detachment of active material from the electrode. The reduction of active material participating in the electrochemical reaction can increase charge overvoltage. Similarly, a loss of porosity (densification) can impede ion transport leading to increases in charge overvoltage. Particularly for the metal hydride electrode, particle size changes have been found experimentally [17, 18, 19, 20] and theoretically [21] to have large effects on the electrode's electrochemical properties and their cycle life [22, 23].
- 2) Burp charging dislodges oxygen bubbles produced on and masking the active nickel electrode surface. Theoretically, it has been shown that displacing masking bubbles augments the effective surface area of the electrode and produces a corresponding reduction in charge overvoltage [24]. Lowering the overvoltage reduces charge heat generation and the tendency for oxygen evolution.

- 3) Burp charging depolarizes the electrode surface by pulling ions away from the electrode surfaces and which ionically agitates the inner Helmholtz plane [25] as a result of a double layer capacitance effect. This agitation facilitates gas diffusion [26].

This thesis is organized in the following manner; Chapter 2 contains the experimental techniques used to demonstrate and understand the performance differences between burp charging and other methods. Chapter 3 contains a discussion of the results of each experimental technique. Chapter 4 summarizes the findings and conclusions of the work.

CHAPTER 2: EXPERIMENTAL

2.1 Performance Cycling

Commercial NiMH 4/3A cells from Sanyo rated at 2400 mAh (P/N HR-4/3AU) were selected for this focused comparison of charge methods because my earlier tests demonstrated their consistent cycling performance relative to competing cell designs. This cell design consists of a foam positive nickel electrode, an AB₅ mischmetal hydride negative electrode, and polypropylene separator. Cells were assembled into 4 cells-in-series packs and cycled 400 times at a C-rate for both the charge and discharge phases. In all cases, the discharge was terminated 1.0V/cell which is considered as 100% depth-of-discharge. Four different charge techniques were evaluated.

- a) Galvanostatic to a maximum temperature (45 °C)
- b) Galvanostatic to a negative voltage slope or a temperature slope (Galvanostatic)
- c) Burp waveform to a voltage inflection point, or a temperature slope (Burp)
- d) Pause waveform is the burp waveform with the discharge pulse replaced by a rest. (Pause)

The control of the burp waveform and termination was achieved using an integrated circuit (IC) named the ICS1702 QuickSaver® [27]. This IC achieved the short discharge pulse by momentarily switching the battery to a calibrated resistor sized to provide about -5A. The pause waveform was achieved by removing this discharge resistor to make the current equal to zero. The galvanostatic waveform was controlled by an IC named bq2003 made by Benchmarq which relies on a negative voltage slope or in a rise in temperature for its termination algorithms. The charger circuits monitored battery temperature with negative thermal coefficient thermistors.

Up to ten battery packs were cycled while in a thermal chamber set at 25 °C. The control of the cycling of each of 10 battery packs was done independently. I developed a computer program to automate the cycling of all the packs. The cycling was operated without interruption for 400 cycles over a six week period. With a C-rate charge and a C-rate discharge and only 5 minute rests in-between transitions, about 10

cycles a day were achieved. Battery voltage, current, and temperature were recorded at about 0.1 Hz throughout the cycling. Voltage and current were measured to ± 1 mV and ± 1 mA resolution while temperature was measured to ± 0.1 °C.

More detailed descriptions of the test articles, test set-up, equipment used, and test conditions of the performance cycling experiments are in Appendix A.

2.2 Cell Calorimetry

Calorimetry was employed to quantitatively determine cell thermal response differences between the various charge methods. After achieving 400 cycles, one of the 4 cells from each pack was separated from the pack in order to place it in the chamber of a Hart Scientific heat conduction calorimeter. Once in place, the cell was reconnected in series with its original pack. One battery pack at a time was cycled with the same charge method as before. In addition to the battery parameters monitored as before, the cell voltage and heat from the cell in the calorimeter were recorded as well. The calorimeter chamber was controlled to 23 °C and maintained within a ± 0.01 °C. Cell voltage and heat were measured to ± 1 mV and ± 0.1 mW, respectively.

The thermal time constant of this calorimeter is about 6 minutes. Thus, to isolate the heat measurements from charging and discharging phases, a two hour rest period followed the charge and a 30 minute rest followed the discharge. This permitted the heat measurement to return to equilibrium before starting the next phase and enhanced the accuracy of area under the curve calculations (i.e. thermal energy). Thirty cycles were performed this way on each battery pack before repeating with the next pack and charge method. Each pack was charged with the same waveform and termination algorithm used to accumulate its previous 400 cycles.

More detailed descriptions of the test articles, test set-up, equipment used, and test conditions of the calorimetric experiments are in Appendix B.

2.3 Destructive Physical Analysis

To investigate the first hypothesis concerning changes in electrode morphology, cycled cells were disassembled in an argon filled glove box to extract active material samples from both electrodes. The samples were examined with Scanning Electron Microscopy (SEM) and Energy Dispersion Spectroscopy (EDS) to visually and elementally compare the surfaces, respectively. Additional analysis included the surface area and pore size distribution of the positive electrode samples and the particle size distribution of the negative electrodes. Samples from cells with 400 burp, pause, and galvanostatic cycles were compared to cells charged once galvanostatically.

More detailed descriptions of the cell disassembly method, of the electrode sample preparation, and of the analysis instrumentation are in Appendix C.

2.4 Video-microscopy

Video-microscopy was used to qualitatively observe changes in cell gassing activity while under the various charging methods. The electrode coil was extracted from its cell can and placed in a transparent beaker. A 6.4 M potassium hydroxide (KOH) solution was used to immerse a ¼ of the coil. That lower portion of the electrode coil had a portion of its outer separator layers and outer hydride electrode cut away to view the nickel electrode with a video-microscope. This was achieved by uncoiling the coil to scissor cut an aperture. Coil compression was regained with Tefzel® tie-wraps. The beaker used was made of transparent polymethylpentene which resists attack from alkaline solutions. Electrical leads were fed through a customized rubber stopper to enable cycling the cell while sealed.

The video-microscope (model PV-10 manufactured by Olympus) and lens system used provided a variable zoom capability from 10X to 70X magnification. The system was connected to a television monitor with a videocassette recorder.

The cell was cycled with each of the three charge techniques (galvanostatic, pause, and burp) while bubble formation on the submerged portion of the coil was observed and recorded. Particular focus was placed on the nickel electrode surface. The current waveforms were controlled and generated by an arbitrary waveform generator. Table 1 describes the waveforms compared. The one second period was extended to 5 seconds to allow more time between pulses to assess a possible cause and effect relationship between the current step change and oxygen bubble formation/dislodgment.

Table 1. Description of waveforms compared during video-microscopic experiments.

Current Waveform	Description	Period (seconds)
Galvanostatic	Constant current of 2A	infinite
Pause	2A interrupted with a 25 ms rest	1
Pause5	2A interrupted with a 125 ms rest	5
Burp	2A interrupted with -5A, 5 ms pulses followed by a 20 ms rest	1
Burp5	2A interrupted with -5A, 25 ms pulses followed by a 100 ms rest	5

A beeper was connected to a voltage comparator to sound an audible beep during each occurrence of a reverse pulse or relaxation period in the current waveform. This sound was recorded by a microphone onto the VCR tape to allow one to determine if a correlation exists between bubble formation (or dislodgment) and current pulse or relaxation. Only qualitative observations were made with this test method.

More detailed descriptions of the test articles, test set-up, equipment used, and test conditions of the video-microscopy experiments are in Appendix D.

2.5 Manometry

Manometry was used to quantitatively measure cell gassing rates and quantities as a result of various charge methods. Pressure variations during cell cycling were measured and recorded with a water filled manometer. A small hole was drilled in the center of the bottom of the can of a commercial cell from Sanyo which had been charged and discharged 10 times. The cell was placed in a 50 ml graduated cylinder and sealed with a rubber stopper. Tubing connected the cylinder to the input end of the manometer. Cell electrical leads were fed through the rubber stopper to enable cycling the cell. The same electrical set-up used in the video-microscope experiment was used for this experiment.

The U-tube of the manometer was filled with distilled water. A vertical displacement of up to 20 cm of water could be accommodated and changes could be measured to within ± 0.025 cm. A rate of gas evolution was calculated by measuring water displacement as fast as every 30 seconds. The manometer was calibrated by introducing a known quantity of nitrogen gas with a syringe into the rubber stopper of the cell.

One ml of gas produced a 4.1 cm displacement of water or conversely, 1 cm displacement results from a 0.244 ml of gas generation.

The cell was charged and discharge twice with each of three charge waveforms; galvanostatic, burp, and pause. The comparison was performed on 3 consecutive days. The first cycle was performed to stabilize the cell. The second cycle was performed immediately after the 1st and is deemed more valid for comparison. To equalize the charge input rates of each method, the galvanostatic portion of each charge sequence was set at slightly different levels. For example, to match the charge rate input of the burp charge at 2A, the galvanostatic and pause charge rate were set at 1.915A and 1.974A, respectively. At these rates, each charge technique achieved the same net charge input per period. In each case, the cell was discharged to 1.000V using a 0.5 ohm resistor and the charge was terminated when cell voltage reached 1.550V.

A second set of comparison tests was conducted to exaggerate possible differences between charge methods. In this case, all three conditions began charging galvanostatically for the first 55 minutes of charge. Thereafter, every minute included a 6 second OCV rest for the exaggerated pause waveform while the exaggerate burp waveform coupled a 1 second 5A discharge pulse with a 5 second OCV rest every minute. The charge current levels for the three waveforms were as follows: galvanostatic (1.915A), pause (1.965A) and burp (1.985A).

A third set of comparison tests was conducted with the cell flooded in 6.4M KOH solution. The objective was to minimize solid-gas recombination reactions 4 and 6 to better measure the electrochemical gasing products from reactions 2 and 5. As in the two previous manometric tests described, the cell coil was not disturbed, only a small venting hole was drilled into each end of the cell casing. The cell was flooded with electrolyte for over a week before cycling to ensured complete electrolyte immersion of the cell coil.

More details on the test article configurations are in Appendix E.

CHAPTER 3: RESULTS AND DISCUSSIONS

3.1 Performance Cycling

Repeated galvanostatic charging NiMH cells to a end temperature of 45°C can hurt cycle life very significantly as shown in Figure 2. Here, a 2.4 Ah cell was charged at C-rate until a set temperature at the cell skin is achieved. After 200 cycles, the C-rate discharge capacity performance of the cell severely degrades. Note that maximum discharge capacity output during the first 200 cycles is about 97%.

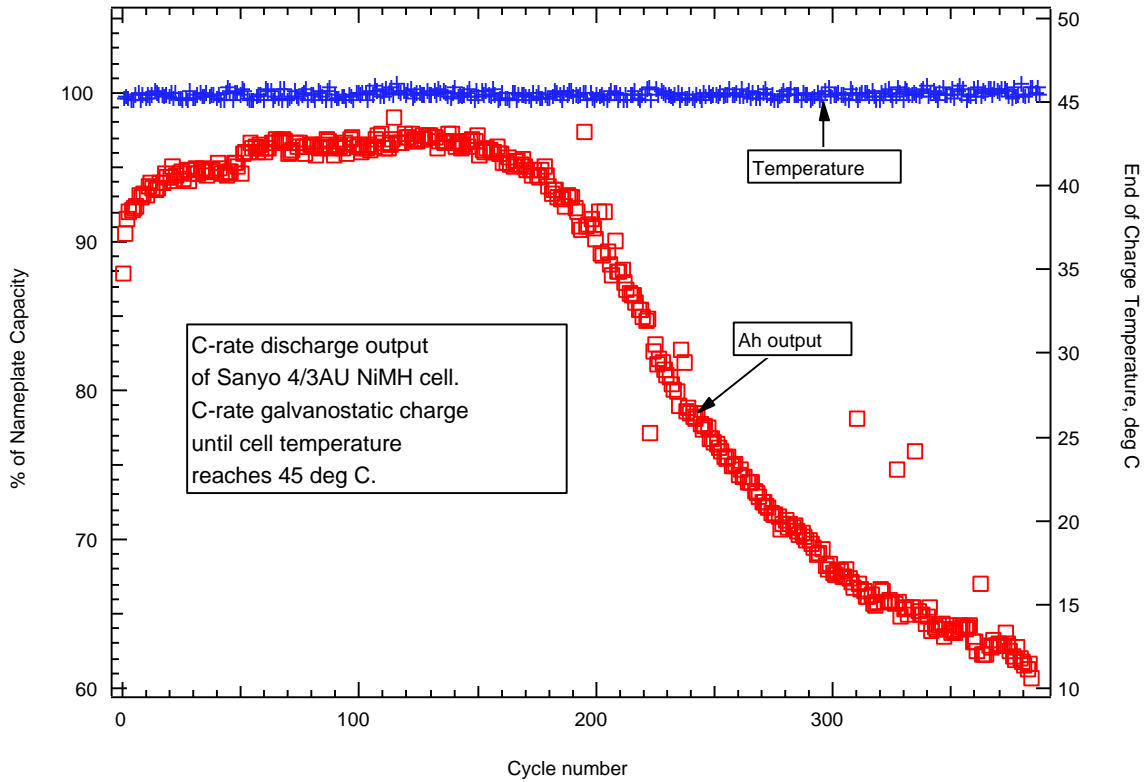


Fig. 2. Simple galvanostatic charging effects on cycle life.

Using the same galvanostatic waveform with a more sophisticated termination algorithm yields a very different result. The charge was terminated when a negative voltage slope or a certain rise in cell temperature were detected. The results in Figure 3 show a more prolonged break-in period before achieving maximum discharge capacity of 99% of nameplate capacity (2.4 Ah) within 250 cycles and remaining

steady to 400 cycles. The end of charge cell temperatures were kept between 30 and 35°C through most of the cycling.

From these results, one can conclude that the “smart” termination algorithms limited the amount of overcharge heat generated every cycle. The cycle life improvement comes at a cost in the output during the early cycles. The break-in period is prolonged.

When the C-rate burp charging waveform of Figure 1 is used, the C-rate discharge output is improved without any detriment to cycle life as is shown in Figure 4. Discharge outputs of 102% were achieved. In addition, the break-in number of cycles to reach outputs of 97% was reduced from 160 to 90 cycles. As with the “smart” galvanostatic method, cell temperatures at the end of charge as measured on the cell skin were maintained below 35 °C. Therefore, the burp method produced a greater sustained discharge output without increasing cell temperature or compromising cycle life.

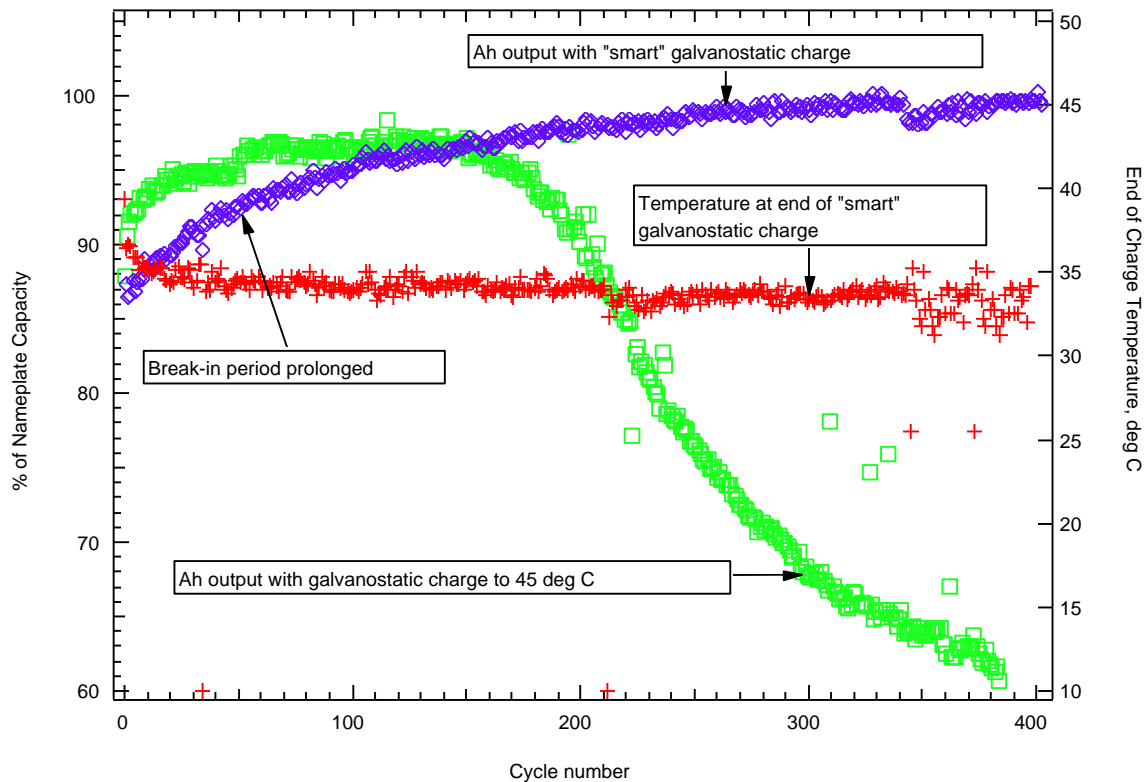


Fig. 3. Smart versus simple galvanostatic charging. Comparison of discharge output versus cycle life.

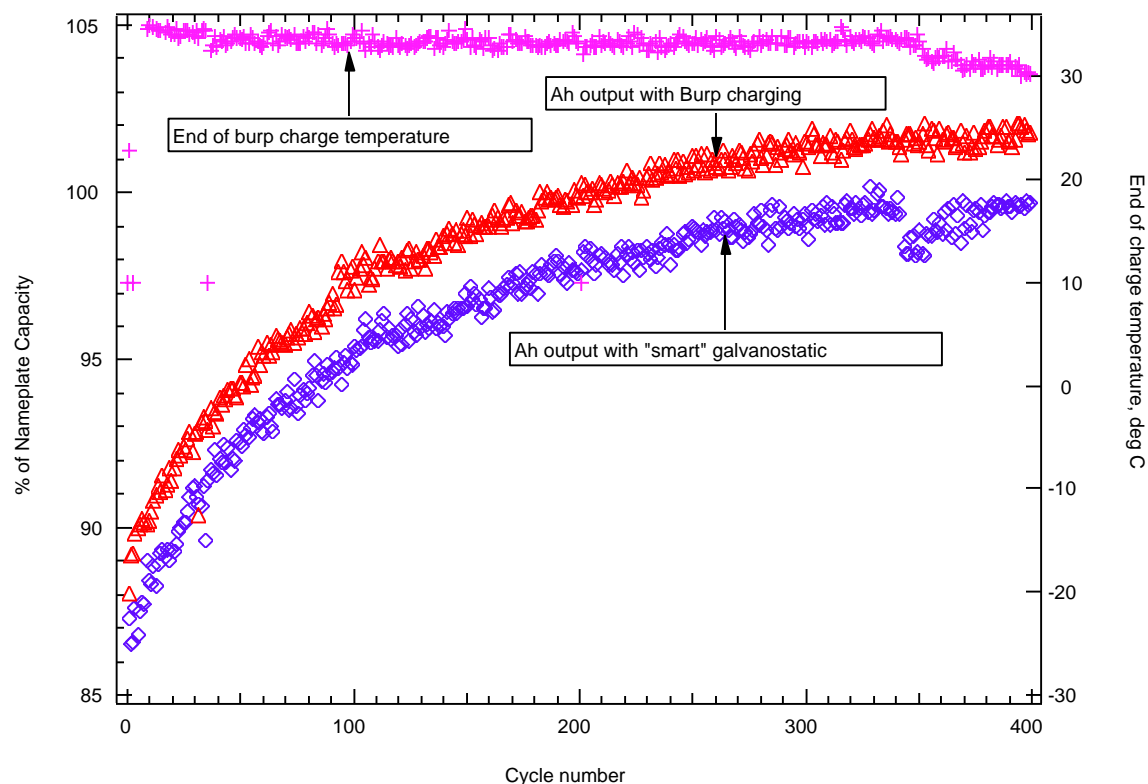


Fig. 4. Burp charging versus smart galvanostatic charging. Comparison of discharge output versus cycle life.

3.2 Cell Calorimetry

These cycling results from the previous section provoked questions as to why and how the performance is improved by the burp current waveform versus the constant current waveform. Do the two methods produce different charge efficiencies, charge overvoltage, and/or charge heat generation rates? What effect does the short discharge pulse have relative to the effect of the following 24 ms rest? Which is more important in improving discharge output and shortening break-in period?

Insights can be obtained from the calorimetric experiments of an individual cell charged galvanostatically and per the waveform in Figure 1 without the discharge pulse. The latter waveform is referred to herein as the pause waveform. From the Figure 5 results, one can see that the charge overvoltage of the two methods overlay on each other except at the beginning and at the end of charge. A closer look at the beginning shows that initially the voltage and heat rise are retarded with the pause waveform. Since the charge portion of the pause waveform was kept at the same current level (2.3A), the Ah charge input per

period for the pause waveform versus the galvanostatic waveform is 3% lower. However, the charge heat is reduced throughout the bulk of the charge by more than 3%, except at the end of charge. Therefore, the reduced charge heat generation by virtue of the pause method can not be attributed solely to its 3% lower charge input per period.

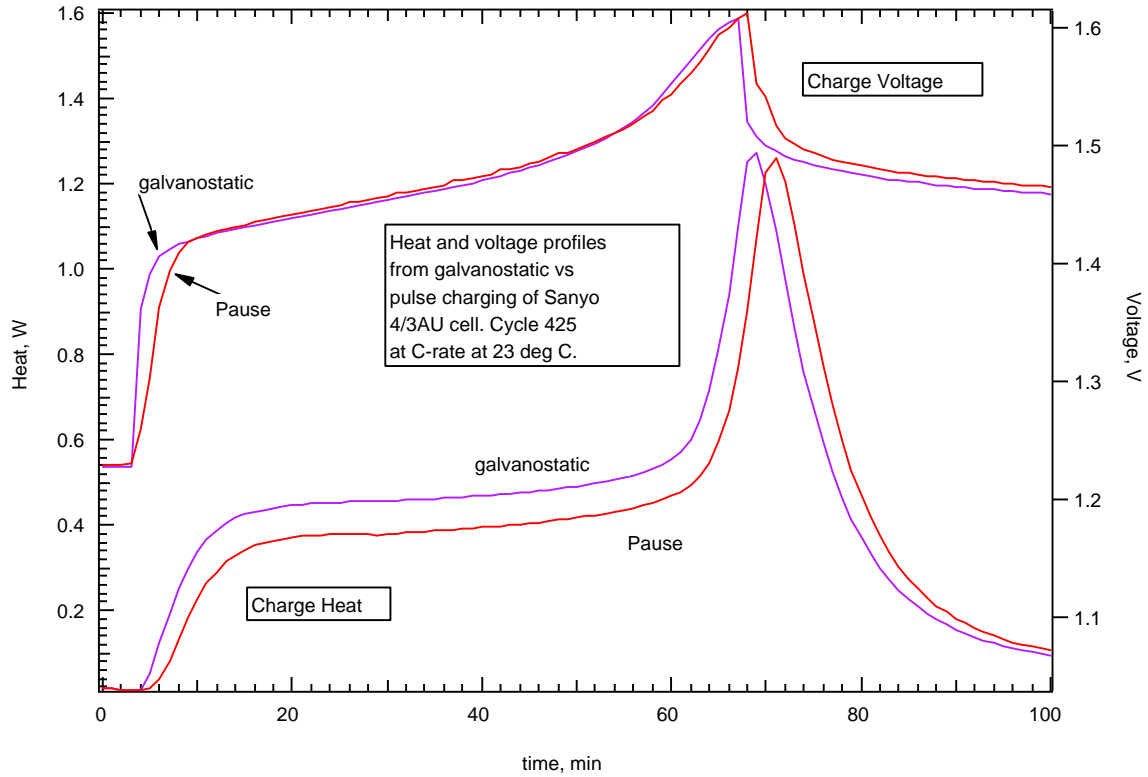


Fig. 5. Calorimetric comparison of galvanostatic and pause charging. Charge heat and voltage comparison versus time.

The peak voltage and heat levels are similar, but the pause peaks occur about a 1 minute later. Most significantly, the charge heat rate in W is reduced throughout the charge with the pause waveform. The area under the heat curve, in J, is about 8% lower than with the galvanostatic waveform. This is unexpected because the charge overvoltages were so similar, and the temperature rise ($T_{\text{final}} - T_{\text{initial}}$) in the cells during charge remained unchanged.

Adding the 5 ms discharge pulse, to obtain the burp waveform, reduces the charge input per period another 1.25% further. It reduces the heat generation rate and the charge overvoltage as shown in Figure 6. Lowering the cell heat generation allowed a greater charge input (in Ah) prior to termination by the same

algorithms as the pause technique. Specifically, a 5% greater charge input was allowed, resulting in a 5% greater discharge output during calorimetric cycling. The most noticeable reason for the greater charge input is the delayed rise in charge overvoltage particularly near the end of charge. The charge heat rate is 6% lower than for the pause waveform at the midpoint of the charge. The temperature rise in the cell was lowered by 1°C, despite the larger charge input in Ah. At the same relative states-of-charge, a difference of nearly 50 millivolts occurred in the charge overvoltage near the end of charge. Therefore, the burp pulse is responsible for lowering the charge overvoltage and heat allowing a greater charge input (resulting in greater discharge output) than can be achieved by the pause method.

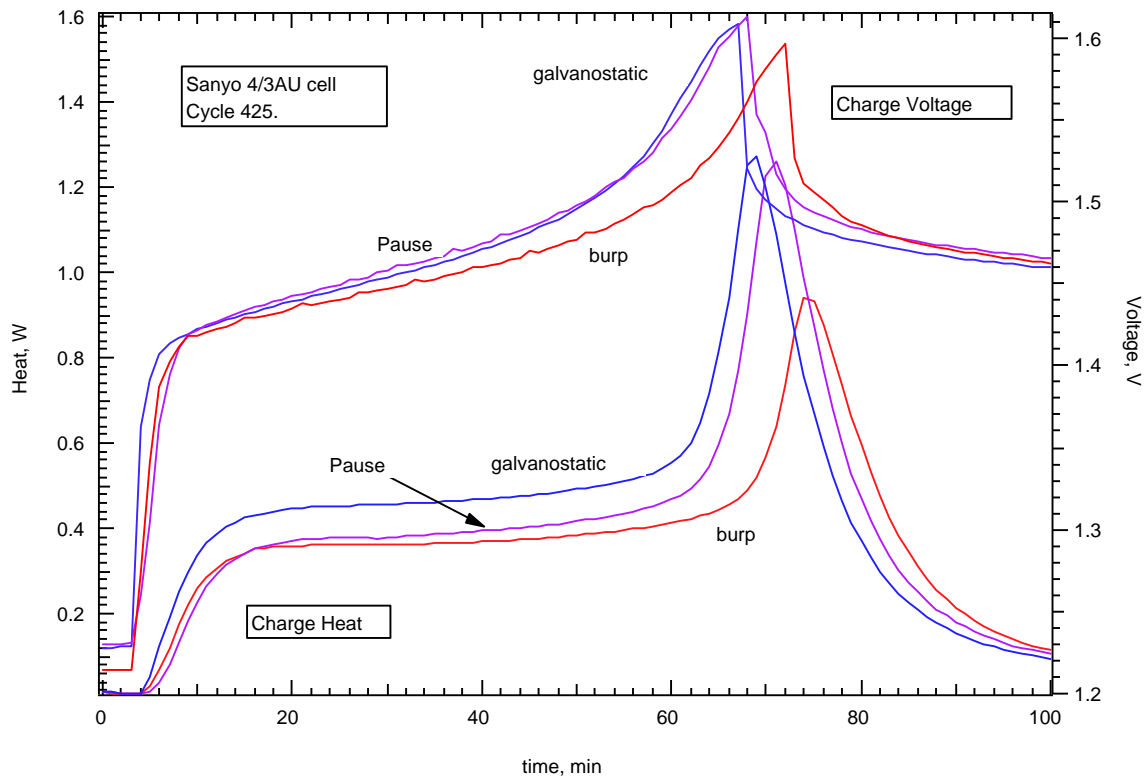


Fig. 6. Calorimetric comparison of the three charge waveforms. Charge heat and overvoltage versus time.

3.3 Destructive Physical Analysis

SEM and EDS revealed these differences between fully charged electrode samples and those charged after 400 cycled times;

- a) The average metal hydride grain size decreased noticeably with all cycling methods.
- b) EDS revealed a mischmetal hydride surface composed of La, Ce, Nd, Pr, Ni, Co, Al, Mn, Zn, with traces of Dy and Sm. More Mn was noticeable on the surface of the 400 cycled hydrides than the once charged hydride.
- c) The once charged nickel electrode surface had a pasted appearance while all the cycled surfaces appeared much more fibrous.
- d) In all the above analyses, differences between the cycling methods were not discernable.

The results of surface area and pore volume analysis of the positive electrodes are shown in Table 2. Surface area decreases and pore volume slightly increases with cycling when comparing the once-charged electrodes to ones cycled 400 times at 100% DOD. Within a 80% confidence interval on the average of the measurements, the burp method does not stand out significantly better than the galvanostatic method to prevent loss of pore volume with cycling. In contrast, the BET surface area difference between the galvanostatic and either the burp or pause method is significant. The transient (burp and pause) methods cause a loss in electrode surface area which indicates that the particle, crystal, or grain size has increased with these methods. This data on cells cycled at 100% DOD is contrary to the hypothesis that burp charging prevents formation of large crystals which reduce surface area. It has been reported that cycling NiMH and NiCd cells with repeated partial discharges, followed by moderate overcharge causes a voltage depression sometimes referred to as a memory effect [28]. The cause of this effect has been linked to a phase conversion of the nickel charged active material from β -NiOOH to γ -NiOOH with a concomitant increase in particle size [29]. In cell cycling studies specifically aimed at examining this phenomena, the burp waveform and its termination algorithm were found to mitigate this voltage depression effect [30]. Therefore, since the work herein did not examine this effect, no validation or contradiction is offered.

Finally, the pore volumes of the control, burp, and galvanostatic electrodes are all within the 80% confidence interval. Only the pore volume increase of the pause method stands out as significant. No explanation is offered for this at this time.

Table 2. Nickel electrode surface area and pore volume comparison

Parameter	Control (charged once)	Galvanostatic	Pause	Burp	80% conf. interval
BET surface area, m ² /g	19.2	17.2	14.4	15.3	± 0.52
Pore volume with dia < 200 nm, cc/g	0.049	0.054	0.065	0.052	± 0.003

The results of particle size distribution of the hydride electrode samples are shown in Table 3. Median and mean are given with a standard deviation along with the range of minimum and maximum particle size. These wide distributions have standard deviations too large to make any conclusions other than the once-cycled hydride has slightly larger grain sizes than all the hydrides cycled 400 times.

Table 3. Metal hydride particle size distribution comparison

Sample	Median (μm)	Mean (μm)	Standard dev. (μm)	Range (μm)
Control (1 charge)	42	47	26.7	2.0 - 229
Galvanostatic	34	40	26.2	2.6 - 229
Pause	34	38	22.3	2.6 - 175
Burp	36	41	26.4	2.3 - 200

Therefore, all these data, obtained on sealed NiMH cells cycled at 100% Depth-of-Discharge (DOD) do not support an electrode morphology mechanism as proposed in hypothesis #1 to explain the burp charge phenomena as found with vented NiCd cells [3]. This suggests that sealing the cell may have a prominent role. Cell pressure effects will be investigated in later sections.

Could double-layer capacitance effects be responsible for the differences in overvoltage observed between the charge methods? A closer look at the transient voltage response during the current interruption of the pause with an oscilloscope reveals a 0.16 V drop per cell requiring 20 μs to fully develop as a result of interrupting a 2 A charge. Therefore, the capacitance effect of the double-layer decays at a much faster rate than the duration of the pause or burp event of these transient charge methods. These results are consistent with previous findings for porous electrodes [31]. This means the period of the burp and pause methods would have been shortened to ~20 μs to potentially benefit from the double-layer capacitance effect.

Thus, double-layer capacitance is not found to be the direct mechanism for the overvoltage effects observed as in hypothesis #3. However, can the effect facilitate gas diffusion? Since the double layer is very thin (~ 1x10⁻⁹ m) and adjacent to the electrode surface, its agitation impact on gas bubbles is restricted to

that thin surface region and can possibly impact the bubble's surface tension. Since this region is smaller than the average pore size ($\sim 30 \times 10^{-9}$ m) of the nickel electrode and much smaller than the average particle size ($\sim 35 \times 10^{-6}$ m) of the metal hydride electrode through which the gas bubbles must diffuse, and the effect decays so quickly, it is not regarded as a prominent factor.

3.4 Video-Microscopy

Video observations at 70X magnification were focused on a portion of the current collector of the nickel electrode which was submerged in electrolyte because that is where the oxygen bubbles are generated. During charge, these revealed a very significant amount of bubble generation whose rate increased with state of charge. During the first 30 minutes of charging at 2 A, very little bubbling activity is noticeable. Thereafter, the bubbling becomes more pervasive. After 45 minutes, some larger bubbles are noticeable as they rise much faster to the surface of the electrolyte level which was set at one quarter up the cell coil. Once 55 minutes into the charge, the largest bubbles appeared and flaking of electrode material was observed. These were accompanied with a steady stream of the small bubbles.

No cause and effect relationship between the occurrence of a pause or burp in current and the release of bubbles could be established. The flow of bubbles is too steady and pervasive throughout the observed electrode. Even when the period of the pause and burp waveform was expanded by a factor of five, no qualitative differences could be discerned with the 5 second period. No video-microscopic evidence was found supporting hypothesis #2 that reverse pulse of burp charging dislodges oxygen bubbles masking the positive nickel electrode surface.

Even after the charging was terminated, the flow of bubbles continued steadily, albeit without increasing. It takes over 1 minute after termination of charge to notice a decrease in bubble flow. Even after resting for one hour, a very small flow of very small bubbles is still observable. However, within one minute of starting a C-rate discharge, one can visually detect that the flow of bubbles has slowed even at the high magnification levels. The response delay to current changes can be attributed to the tortuous bubble path present in these porous electrodes.

Clearly from these observations, the gas evolution reactions play a significant role during charge. The role apparently increases non-linearly with increasing state-of-charge. Furthermore, the onset of

discharge also produces a gas consuming effect which is visually detectable. This provides an insight that gas consumption may be also occurring during the burp pulse during charge. An alternative experimental method is required to quantify the gas evolution amount and rate with the various charge methods.

3.5 Manometry

In the manometric set-up, the cell was least disturbed from its commercial configuration. The electrode coil was still under its designed compression level inside its cell can and with its original electrolyte quantity and composition. The only cell level changes versus the calorimetric experiments were that its pressure at 0% state-of-charge was zeroed to ambient pressure before beginning the nearly C-rate charge and that gases generated had a bigger volume to expand into, which maintained cell pressures at lower levels. Therefore, the chemical and electrochemical equilibriums were not the same.

From Fig. 7, one can see that the gas evolution curves show an exponential increase near the end of charge as was qualitatively discerned from the video-microscopy observations. The shape of the galvanostatic gas curve is similar to that recently determined by others experimentally [11, 32] and predicted theoretically [33]. At this current rate, significant gas evolution occurs with all methods well before reaching full charge and the majority of constituent is hydrogen, not oxygen [11, 32]. Therefore, the effects the various waveforms have on the hydride electrode and its reactions can not be dismissed compared to the effects on the nickel electrode in contributing to the cell pressure.

The galvanostatic charge method resulted in significantly more gas generation near the end of charge than either the burp or pause method. Fifty minutes into the charge, the gas generation rate of the galvanostatic method diverts from the other two methods. At the time the galvanostatic method had reached the cut-off voltage of 1.550V (73.5 minutes into the C/1.2 charge), the galvanostatic method had generated twice the gas volume as the other two methods while receiving equivalent charge inputs in

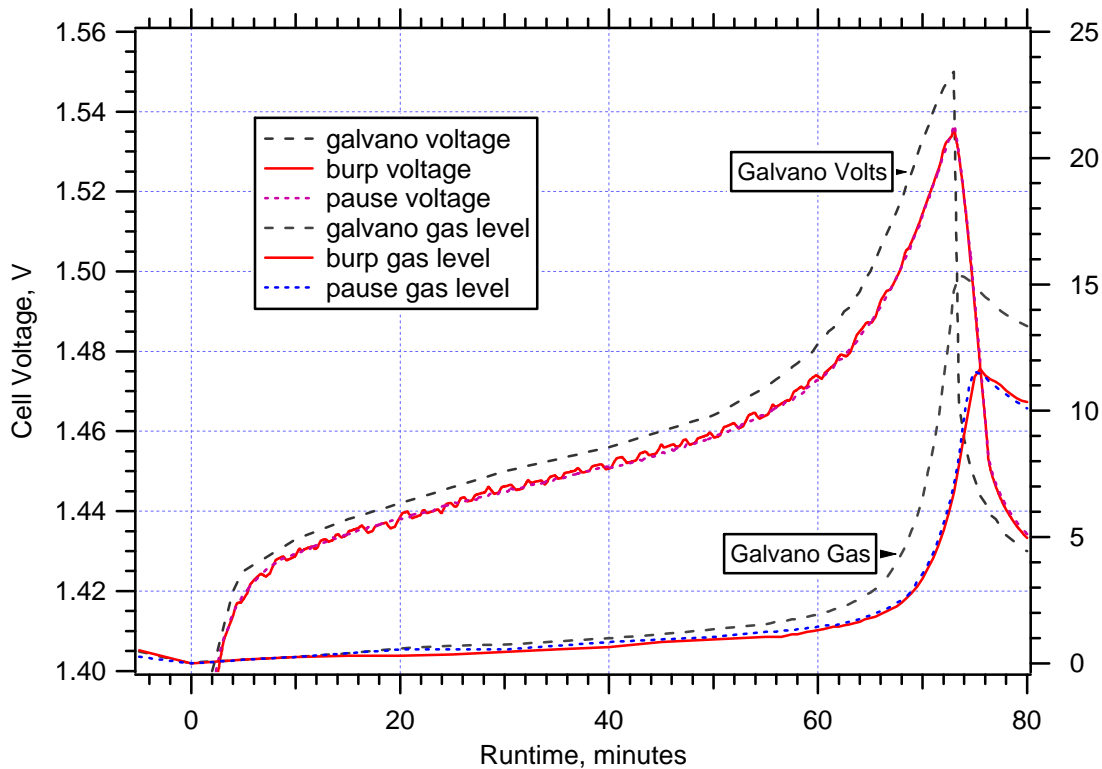


Fig. 7. Comparison of the charge overvoltage and gas generation of three charge methods (burp, pause, and galvano) versus runtime with the same nickel metal hydride cell. Initiation of 2nd charge/discharge cycle for each method was at a runtime of 0 minutes. Gas generation volume indicated by centimeters of water displaced in a manometer. Current levels; Burp at 2.000A, Pause at 1.974A, Galvano at 1.915A.

ampere hours. In contrast, very little difference exists between the pause and burp gas curves. One can infer from this result, that interrupting the galvanostatic charge is more important than also including a discharge pulse (burp).

The charge overvoltage values from the curves are quantitatively about 10 mV higher at comparable states of charge to the values from curves shown in Figs 5 and 6. An ohmic losses error analysis of the calorimetric and manometric test cells determined that, for both cases, of the overvoltage difference is strictly due to a combination of not being able to run at the same test current (2.0A vs. 2.3A) and not being able to place voltage sense leads directly on the cell terminals. Details of this analysis are in Appendix E. Nevertheless, the charge overvoltage curve of the galvanostatic method also followed a similar pattern relative to the overvoltage of the other methods. From the onset of the charge, the galvanostatic overvoltage curve is higher than the other two. This causes the galvanostatic charge to reach the cut-off voltage about

1.75 minutes sooner than the other two techniques. This was also observed upon analysis of the results of the performance and calorimetric cycling experiments. Thus, interrupting the galvanostatic waveform with rest or with rest and burps, lowers the charge overvoltage.

However, it is surprising to not see any significant overvoltage or gas evolution differences between the burp and pause methods in Figure 7. The differences in the charge overvoltage curves between burp and pause in Figure 6 were not replicated in Figure 7. A main difference between the manometric and the calorimetric cells is that the operating pressure of the cell was much lower for the manometric test because a hole had been drilled into it to connect it to the manometer. The inert volume of the manometric cell is estimated at over 100 times that inside the undisturbed cell used during the calorimetric test. Therefore, the partial pressure of hydrogen and oxygen is correspondingly less for the manometric cell. Why the reduced partial pressure mitigates the charge voltage and gas evolution differences between the burp and pause waveforms is unknown.

A smaller difference is the charge current level. The calorimetric tests used the same 2.3A charge current for each method. Burp charging at 2.30A is equivalent to pause charging at 2.27A at an equivalent charge input per period. However, this small current change can only account for less than 1 mV of difference based on a 22 mohm cell internal resistance estimated from voltage fluctuations during step changes in current [34] in a method similar to that used previously [35]. In contrast, the burp and pause waveforms diverged by 10 mV at the mid-charge point in Figure 6. Therefore, the slight variation in charge current level do not invalidate the results.

The goal of the exaggerated waveform test was to determine if lengthening the period of the waveforms would produce a more discernible difference in the overcharge and gas evolution results. The waveforms were all galvanostatic until 55 minutes into the charge. Up to that point, the overvoltages of all three curves varied by no more than 4 millivolts and manometer levels were within 0.3 cm of each other. Thereafter, the overvoltage curves separated slightly while the gas curves diverged more significantly. In Fig. 8, the overvoltage data of the transient methods are displayed without smoothing the data for clarity with a moving average box car algorithm as is done in all other figures. Note that with data recorded roughly every 2 seconds, voltages at different stages of the waveforms are recorded yielding what maybe misinterpreted as measurement noise.

At the end of charge, the order of decreasing overvoltage was galvanostatic, pause, and burp as was found in the calorimetric cycling. Similarly, after 65 minutes into the charge, the order of decreasing rate of gas evolution was galvanostatic > pause > burp. This experiment helped distinguish the advantage of the burp over the pause method.

In this test, the burp overvoltage took the longest to get to the cut-off voltage of 1.550V. The onset of the exaggerated pause causes a temporary reduction in overvoltage relative to the galvanostatic method. However, this effect is not long lasting as the two methods reach the cut-off voltage at the same time. Nevertheless, the pause method does retard gas generation relative to the galvanostatic method. The pause method temporarily reduces the overvoltage while the full second discharge pulses of the exaggerated burp method produced a more lasting overvoltage reduction. The burp method is best at retarding gas generation. Figs. 7 and 8 demonstrate a correlation between higher overvoltage and higher gas generation.

The pause waveforms of Figs. 7 and 8 are nearly identical. This indicates that a five fold extension the relaxation time step (from 30 to 150 milliseconds) does not lower the gas generation rate. Therefore, lengthening the pause time does not produce any benefit. In contrast, a comparison of the burp waveforms, indicates that lengthening the discharge pulse of the burp method from 5 to 25 milliseconds does reduce or retard the gas generation rate.

Furthermore, saving the pause and burp steps towards the end of the charge as in Fig. 8 appears to be just as effective as having them throughout the charge process as in Fig. 7. This suggests that an improved charge could be attained by making the frequency and the length of the burp and relaxation steps increase as a function of increasing state-of-charge. Additionally, this is more evidence that a gas related phenomena is more likely responsible than a changing electrode morphology phenomena as proposed in hypothesis #1. It is difficult to understand how a morphological phenomena could have a similar variation with state-of-charge.

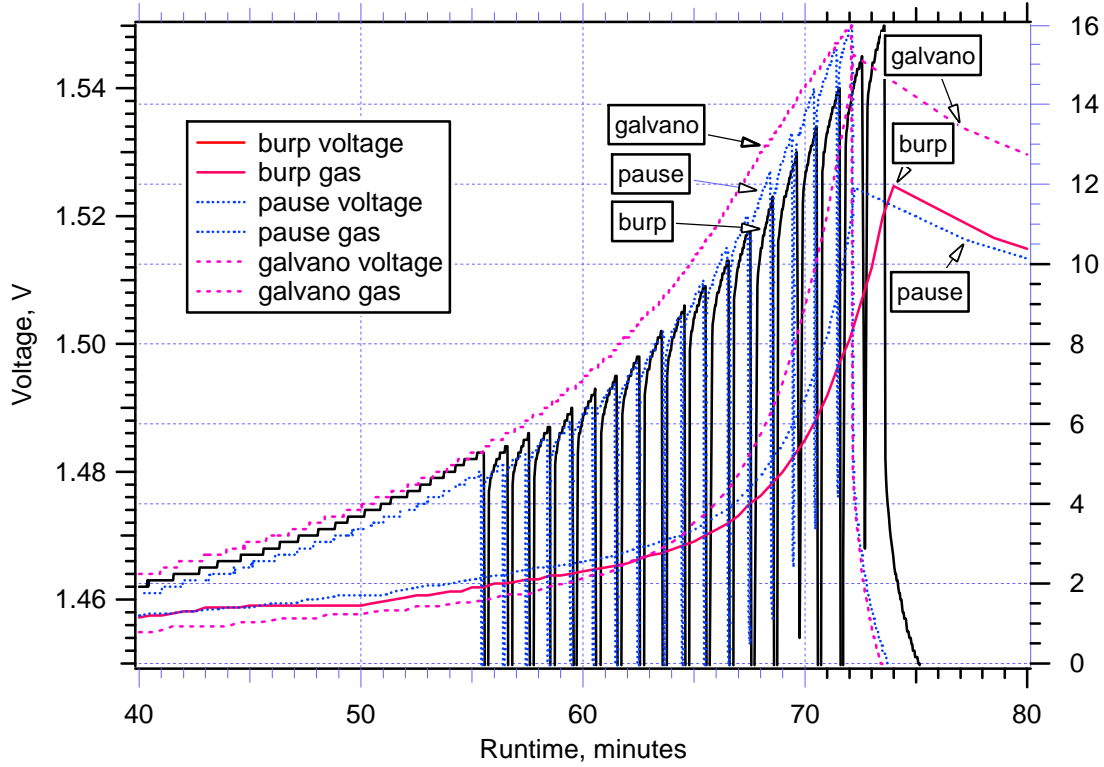


Fig. 8. Comparison of the end of charge with exaggerated pause and burp waveforms versus runtime with the same nickel metal hydride cell. Initiation of the charge was at a runtime of 0 minutes.

Figure 9 shows a typical gas curve during the very end of charge and throughout charge rest and discharge. Thirty seconds after the end of charge, gas evolution peaks and non-linearly decreases thereafter. The decrease during the charge rest is due to the chemical reactions of oxygen and hydrogen gas recombination via



oxygen recombining with surface hydride (reaction 4), and hydrogen hydriding at the negative electrode via,



Note that at the onset of discharge, the rate of gas consumption (slope of the gas curve) becomes noticeably more negative indicating an increase in gas consumption. This was also observed during the video-

microscopic experiment. Flow of small gas bubbles from the nickel electrode nearly disappear after the onset of discharge.

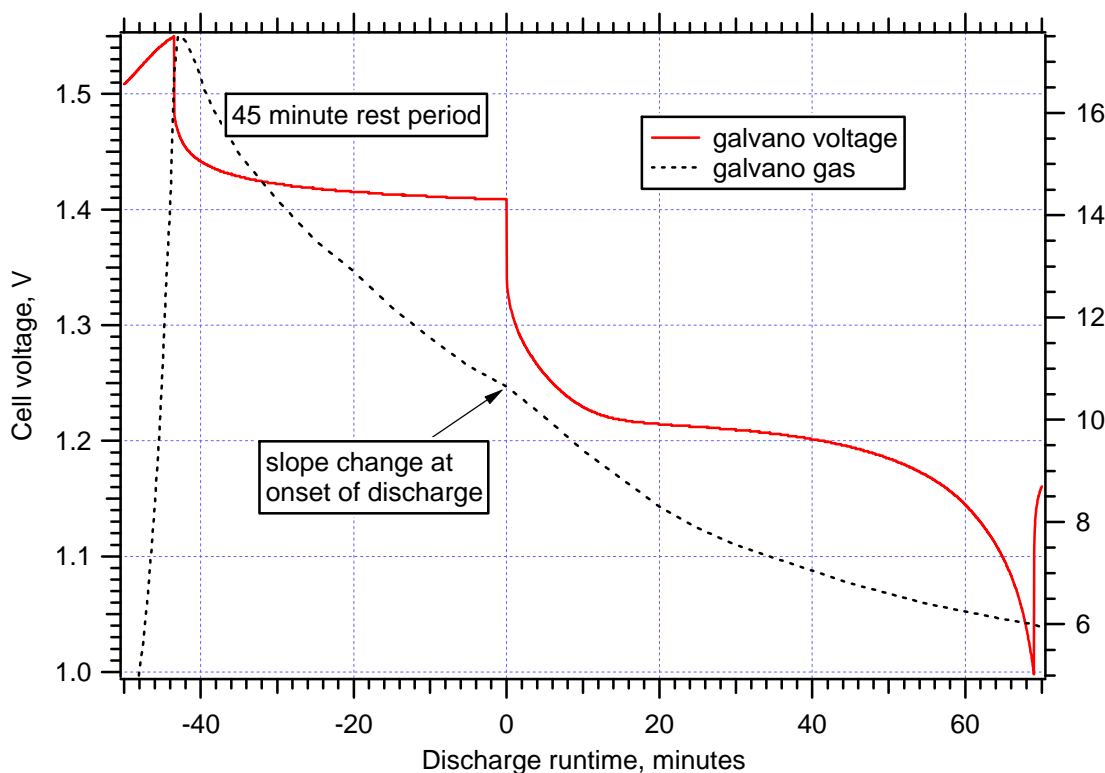


Fig. 9. Voltage and gas evolution curves versus runtime during a charge rest period followed by cell discharge into a 0.5 ohm load.

These observations support the mechanism that during the discharge pulse of the burp waveform, oxygen bubbles are not dislodged but rather consumed at the positive electrode surface. During this burp pulse, two competing electrochemical options exist; one is the reverse of the half-reaction 1, the other, the reverse of half-reaction 2. Envisioning a charged pore surface of the positive electrode with a masking oxygen bubble, which of these two mechanisms will the bubble prefer? One can rationalize that the gas bubble will impede water transport to the NiOOH surface (impeding the reverse of reaction 1) and cause the water to prefer reacting with the masking oxygen bubble (reverse of reaction 2).

At the hydride surface, during the burp pulse, the choices are the reverse of reactions 3 or 5. As was reported previously [10, 11, 14], the reverse of reaction 3 involves diffusion of adsorbed atomic hydrogen from the bulk of the hydride metal structure. This is slower than the reverse of reaction 5 which is a surface reaction. Therefore, a high rate pulse of discharge current (burp) should favor reversing reaction 5

over reversing reaction 3 on the metal hydride surface, which lowers cell pressure by consuming gas. Thus, evidence suggests that gas bubble consumption occurs electrochemically at both electrodes during the rapid discharge pulse of the burp charge method.

The chemical recombination mechanism of reaction 9 requires the transport of the oxygen from the positive to the negative and is very exothermic (-136 kcal/mole of O₂) [36]. If it is prominent, it significantly raises the operating temperature of the cell. Raising the temperature of the metal hydride drives more hydrogen out to recombine with electrochemically evolved oxygen. Via this chemical process, the temperature of a fully charged or overcharged cell could continue warming even while it rests on open circuit after charging has stopped. This has been observed while leak testing a competing commercial cell design after placing large groups of closely packed cells in a 50 °C oven immediately after charging the cell at C/10 for 16 hours. Such cells are typically at 32-40 °C as a result of the overcharge. Once open-circuited and placed in the oven, they were found to overshoot the oven set-point [37]. These observations provide some supporting evidence for occurrence of this chemical recombination mechanism at higher temperatures.

Using the following assumptions derived from my calorimetric data, DPA data, and an extrapolation from literature data [11]: 4 atm partial pressure of oxygen after the C/10 charging, 2 cc of void volume in the cell, 0.20 cal/g-°C, 52 g/cell, 40 °C cell temperature, and the ideal gas law, a cell adiabatic temperature rise of 4 °C is predicted as a result of gaseous recombination. Higher temperatures drive more hydrogen out of the hydride and will cause oxygen bubbles trapped in the positive electrode (leftover from the slow overcharge) to expand, which favors their escape. In turn, more reactants will increase the rate of recombination making possible a vicious cycle when closely packed cells can not reject this heat.

In the absence of discharge pulses (“burp”) during the charge, cell pressure is maintained by the chemical recombination processes (reactions 4 and 9) and rehydriding of hydrogen gas at the negative electrode (reaction 10). Adding discharge pulses, adds additional electrochemical mechanisms to consume the oxygen and hydrogen evolved via the reverse of reactions 2 and 5. Removing bubbles from an electrode surface increases its effective area and reduces its local current density. As a result, the overvoltage is

slightly reduced which allows a slightly greater charge runtime. In turn, a lower charge overvoltage results in lower cell heat generation which in a virtuous cycle will reduce oxygen and hydrogen evolution.

In the flooded cell experiment, both electrodes are immersed in liquid electrolyte. The purpose of this experiment was to gain insight on the relative importance of the chemical gas recombination path versus the electrochemical gas consumption path. Since the chemical path requires oxygen transport from the positive to the negative electrode, flooding should make that transport less facile and cause a greater accumulation of gas bubbles near the electrode surfaces.

With the flooded charge process, the lack of solid-gas interfaces impedes the solid-gas reactions (4, 9, and 10) all of which consume gas. As a result after 40 minutes of charging, gas generation rates and amounts are higher as shown in Fig. 10, which compares the nominal (or electrolyte starved) cell data from Fig. 7 to that of a flooded cell during galvanostatic charging. Several features of the flooded cell gas curve are noteworthy. The measured gas level actually decreases very slightly during the early stages of charge and then rapidly begin to rise at a lower state of charge (~ 50% vs 80% SOC calculated on a 2.4 Ah coulombic basis) than for the starved cell. Note that at the beginning of charge, the charge overvoltage of the flooded cell is significantly lower than the starved cell. This is attributed to the increased ionic conductivity resulting from a completely wetted path between electrodes. The increased slope of the charge overvoltage of the flooded versus the starved cell may reflect the loss of that increased conductivity by the emerging transport difficulties associated with the accumulation of surface gases. Coincidentally, once the charge overvoltage of the flooded cell surpasses that of the starved cell (after 30 minutes or at 42% SOC), its gas generation rate rises dramatically. These results confirm the prominent role that the availability of exposed solid electrode surface has on cell pressure by promoting solid-gas interface reactions which consume gas.

The charge of the flooded cell was terminated after 52 minutes of charge to prevent gas levels from exceeding the measurement capacity of the manometer after charge is terminated. Note how rounded the gas curve is after charge is terminated. Peak gas generation lags 20 minutes behind and the gas level increases by 2.5 cm (versus a 30 second lag and an increase of only 1 cm for the starved cell) after charge is terminated. In comparison, once charge is terminated on a starved cell, gas levels lower quickly. This difference reflects the slow nature of gas transport from the pores of the immersed electrodes.

Further evidence of the slowed chemical recombination processes is how much slower gases are consumed during the charge rest and discharge periods. Additionally, as with the starved cell, the onset of discharge slightly accelerates gas consumption. This is more evidence that gases are consumed during the discharge pulse of the burp waveform.

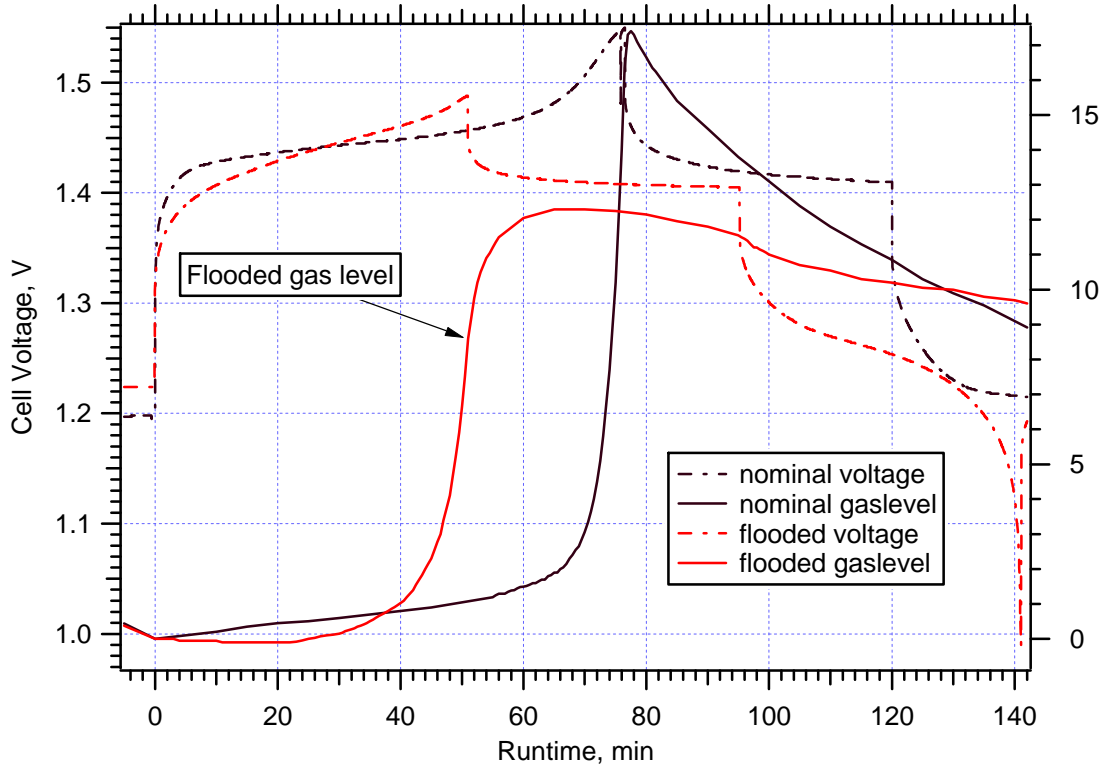


Fig. 10. Comparison of voltage and gas levels in a flooded and nominal cell during galvanostatic charge at 1.915A, rest, and resistive discharge at 0.5 ohm.

The flooded cell experiment also permitted measuring a net cell coil expansion of 0.38 cm^3 which occurs during charge and is manifested by a rise in the immersing KOH level. A net expansion occurs because the expansion of the metal hydride is greater than the contraction of the nickel electrode (where the uncharged species is less dense than charged species [4, 38]). This expansion leaves more room for gas storage and maybe the reason the gas level on the manometer initially decreases after the onset of charge. This effect is small and is soon overwhelmed by the gas generation rate.

Figure 11 shows the voltage and gas levels of all three charge methods applied to the flooded cell. In comparing the gas levels after 50 minutes, the order of increasing gas generation is burp < galvanostatic

< pause (4.80 cm < 6.65 cm < 7.30 cm). The difference between the burp and galvanostatic method, 1.85 cm is much less than the factor of two difference seen for the starved cell before its end of charge point (see Fig. 7). Furthermore, the voltage traces are not discernibly different with each method. Unfortunately, the flooded cell charging process had to be terminated sooner, possibly before differences may have developed.

Nevertheless, the burp method produced the lowest gas curve. A repeat of this test produced very reproducible results. The advantage that pause charging had over galvanostatic charging with the starved cell is not manifested in the gas curves the flooded cell of Fig. 11. This indicates that pause method needs exposed electrode surfaces and facile gas transport to manage cell gas generation better than the galvanostatic method. The short relaxation step of the pause method is not enough to allow diffusion of oxygen bubbles away from the nickel electrode surfaces. Therefore, flooding the cell served to elucidate differences between these dynamic charge methods by slowing gas transport, limiting solid-gas interfaces, and impeding its reactions.

Once the gas consuming chemical reactions are suppressed by the transport limitations of oxygen in the flooded condition, the electrochemical gas consumption surface discharge reactions (reverse of reactions 2 and 5) produce an accumulative effect significant enough to quantitatively measure manometrically. This is more evidence supporting a gas consumption mechanism during the discharge pulse rather than a dislodgment mechanism. If the discharge pulse of the burp method was dislodging gas from the electrode surfaces as in hypothesis #2, the diffusion limitations of the gas in the flooded environment would cause an accumulation of gas near the electrode surface, further impede ionic flow, and raise overvoltage. This was not observed during charge in the video-microscopic or manometric experiments.

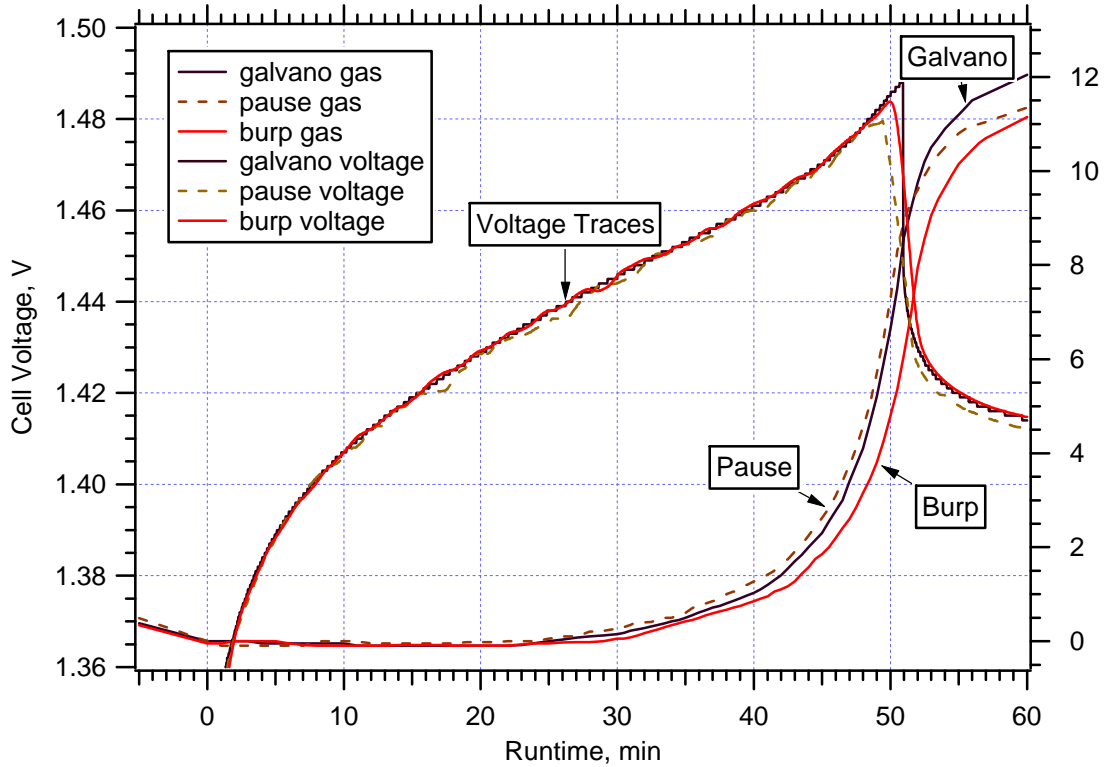


Fig. 11. Cell gas and voltage level during charging of a flooded NiMH cell. Comparison of galvanostatic, pause, and burp charge methods.

What cell and charger design improvements does the results of this work suggest?

As far as the cell is concerned, electrolyte quantity is critical. Too little results in higher ionic impedance. Too much impedes the cells gas management processes. Maintaining a sufficient amount of exposed hydride to support the gas management processes is critical. Reducing the gas transport path by reducing the electrode and/or separator thickness and increasing their area would improve the gas management process. The higher surface area cell could then support higher current rates without a concomitant cell pressure increase. Furthermore, this work indicates that the gas consuming hydride electrode plays an important role in influencing cell pressure and charge overvoltage by virtue that it contains most of the solid-gas interfaces. One should find ways to improve the surface rehydriding kinetics of the hydride to maintain lower hydrogen partial pressures. Additionally, if the inner surface of the can could be coated with a recombination catalyst as exists in aerospace Ni/H₂ cells [4], cell pressures could be better managed.

As far as charger design suggestions, this work indicates that a benefit could be gained from increasing the frequency of the discharge pulses with increasing state of charge. The results of the starved cell with nominal and exaggerated waveforms (Figs. 7 and 8) indicate that not much is gained from the burp pulses during the first half of the charge process and some benefit can be obtained from introducing them as late as after 76% SOC, when they are more beneficial. Similarly, it may be beneficial to increase the duration of the discharge pulse with increasing state of charge. Lastly, the exaggerated waveform experiment indicates that lengthening the duration discharge pulse is beneficial while that of the pause step is not.

CHAPTER 4: SUMMARY AND CONCLUSIONS

In summary, the cycling performance tests on commercial sealed NiMH cells demonstrated that burp (reverse pulse) charging improves cycling capacity without degrading cycle life over pause and galvanostatic methods. In-situ calorimetric tests concluded that burp charging lowers charge overvoltage and heat generation when compared to the other methods. Destructive physical analysis of both electrodes by SEM and EDS revealed no significant differences in active materials cycled 400 times by either techniques. Same conclusion on the particle size analysis of the metal hydride electrodes. Pore volume analysis of the nickel electrode revealed that burp charging maintains pore volume only very slightly better than galvanostatic charging.

In-situ video-microscopy qualitatively revealed the significance of gas-generating side reactions during charge. Focusing on the positive nickel electrode, bubble generation was observed to have a non-linear relationship with increasing state-of-charge. Even with a 70X magnification and an exaggerated pause and burp waveform with a period extended by a factor of five, no cause and effect relationship between the occurrence of a pause step or a burp pulse in current and the release of bubbles could be visually established. However, after a 1 hour charge rest, a very small flow of bubbles are still observable on the positive electrode surface. Within one minute of the onset of C-rate discharge, a reduction in the flow of bubbles is visually detectable. This indicates that the onset of discharge consumes gas.

Manometric gas analysis of cells during cycling allowed for a quantitative comparison of the amount and rate of gas generation or consumption with the various cycling methods. With a normal cell, with little free electrolyte, the burp and pause charge methods generated significantly less gas than the galvanostatic method. With the cell in a flooded state, all the methods produced more gas at earlier states of charge because of less facile gas transport and the lack of exposed hydride to catalyze gas consumption reactions. In flooded cells, pause charging loses its advantage over the galvanostatic method. In the flooded condition, burp charging stands alone with lowest gas generation rate. Gas recombination paths that were facilitated by the pause method in the starved cell are impeded by the slow transport of gases to the hydride electrode in the flooded condition. Burp charging is the only one of the three methods capable of consuming

electrode surface gas by reversing the gas generation electrochemical reactions during the discharge “burp” pulse. Hence, the “burp” label implying a dislodgment of gas is a misnomer and the method is more accurately labeled as “reverse pulse” charging.

As a result of this work, specific cell and charger design recommendations were made. A particular important cell design suggestion, is to maximize the amount of exposed solid surfaces that are catalytic to oxygen and hydrogen recombination. An important charger suggestion would be to increase the frequency and duration of the discharge pulses during charge as a function of increasing state-of-charge.

Conclusion 1: In sealed NiMH cells, it has been demonstrated that during charge undesirable gas generating side reactions and heat increase with increasing charge overvoltage. Charge methods which lower overvoltage maintain lower cell pressures and temperatures. Transient current charge methods such as reverse pulse charging have this advantage over galvanostatic charging with NiMH cells.

Conclusion 2: The video-microscopic and manometric analysis of the cell gas generation and consumption rates support that the reverse pulse or discharge pulse of “burp” charging causes a consumption not a dislodgment of surface gas bubbles via a reversal of the electrochemical gas evolution half-reactions at both electrodes.

5.0 REFERENCES

- [1] F. Benjamin, *SMPTE Journal*, **86**, 204 (1977).
- [2] F. Benjamin, The Reflex Principle of Charging Nickel-Cadmium and Other Batteries, Gardena: Christie Electric Corp., 1972, pg. 3-11.
- [3] O.C. Wagner and D.D. Williams, *Proc. of the 26th Power Sources Conf.*, Cherry Hill, NJ, (1974), p. 96.
- [4] D. Linden, in *Handbook of Batteries*, McGraw-Hill, NY, 1995, section 6.2
- [5] G.S. Nagarajan and J.W. Van Zee, *Journal of Power Sources*, **70**, 173 (1998).
- [6] Y. Sone, H. Kusawake, K. Koga, and S. Kuwajima, "Status of Nickel Metal Hydride Cell Development", 1997 NASA Aerospace Battery Workshop, p. 161.
- [7] A.H. Zimmerman, in *Hydrogen and Metal Hydride Batteries*, P.D. Bennett and T. Sakai, Editors, **PV 94-27**, p. 268, *The Electrochemical Society Proceeding Series*, Pennington, NJ (1994).
- [8] A.H. Zimmerman, *Power Sources* 12, T. Keily and B.W. Baxter eds., Taylor and Francis Ltd., Basingstoke, England, 1988, p. 235.
- [9] T. Fuller and J. Newman, *Modern Aspects of Electrochemistry*, Number 27, R. White, editor, p. 359, Plenum Press, NY, 1995.
- [10] C. Iwakura, M. Matsuoka, and T. Kohno, *J. Electrochem. Soc.*, **141**, 2306 (1994).
- [11] M. Ikoma, S. Yuasa, K. Yuasa, S. Kaida, I. Matsumoto, and C. Iwakura, *Journal of Alloys and Compounds*, **267**, 252 (1998).
- [12] Q.M. Yang, M. Ciureanu, D.H. Ryan, and J.O. Strom-Olsen, *J. Electrochem. Soc.*, **141**, 2108 (1994).
- [13] Q.M. Yang, M. Ciureanu, D.H. Ryan, and J.O. Strom-Olsen, *J. Electrochem. Soc.*, **141**, 2113 (1994).
- [14] P.H.L. Notten and P. Hokkeling, *J. Electrochem. Soc.*, **138**, 1877 (1991).
- [15] B. Kerridge, *Electronic Design News*, 13 May 1993, pg. 100.
- [16] C. B. Falcon, U.S. Pat. 5,600,226, (1997).
- [17] Z. Zhaoling and S. Dongsheng, *J. of Alloys and Compounds*, **270**, L7 (1998).
- [18] T. Ikeya, K. Kumai, and T. Iwahori, *J. Electrochem. Soc.*, **140**, 3082 (1993).
- [19] T. Sakai, A. Uchiyama, H. Miyamura, N. Kuriyama, and H. Ishikawi, *J. Electrochem. Soc.*, **140**, 2450 (1993).
- [20] A. Zuttel, F. Meli, and L. Schlapbach, *J. of Alloys and Compounds*, **221**, 207 (1995).
- [21] M. Viitanen, *J. Electrochem. Soc.*, **140**, 936 (1993).

- [22] F. Meli and L. Schlapbach, *J. of Less Common Metals*, **172-174**, 1257 (1991).
- [23] A. Zuttel, F. Meli, and L. Schlapbach, *J. of Alloys and Compounds*, **200**, 157 (1993).
- [24] J. Dukovic and C.W. Tobias, *J. Electrochem. Soc.*, **134**, 331 (1987).
- [25] F. Williamson, "Battery Management System - Optimized Electrokinetics Control in Galvanic, Electrolytic, and Storage Operating Modes", 1997 NASA Aerospace Battery Workshop, p. 29.
- [26] M. Mankikar, *Electronic Engineering Times*, CMP Publications, Manhasset, NY, (25 July 1994).
- [27] QuickSaver® is a registered trademark of Galaxy Power, Inc., Valley Forge, PA.
- [28] K. Takeno, K. Ikeda, N. Shiojima, H. Hasebe, and Y. Sato, Abstract of 31st Battery Symposium, Japan, p. 157 (1990).
- [29] Y. Sato, K. Ito, T. Arakawa, and K. Kobayakawa, *J. Electrochem. Soc.*, **143**, L225 (1996).
- [30] D. Whitmer, Galaxy Power, Inc., 1998, private communication.
- [31] C. Lagergren, G. Lindbergh, and D. Simonsson, *J. Electrochem. Soc.*, **142**, 787 (1995).
- [32] D. Kim, H. Lee, K. Jang, and J. Lee, *J. Electrochem. Soc.*, **145**, 3387 (1998).
- [33] W.B. Gu, C.Y. Wang, and B.Y. Liaw, *J. Electrochem. Soc.*, **145**, 3418 (1998).
- [34] B. Strangways, "28V CRV Cell Test, Performed for NASA-JSC", SRI report #78J, Jan 1998.
- [35] R. Pollard and J. Newman, *J. Electrochem. Soc.*, **128**, 491 (1981).
- [36] R. N. Smith and C. Pierce, "Solving General Chemistry Problems", WH Freeman and Co. CA, 1980, p. 227.
- [37] B. Strangways, Symmetry Resources, Inc., 1998, private communication.
- [38] Handbook of Chemistry and Physics, CRC, Cleveland, OH, (1966).

6.0 APPENDIX A

Design, Specifications, and Operation of the Performance Cycling Experiment

Overview

An Automated Battery Cycler capable of independently controlling the cycling of 10 batteries was designed and assembled at the National Aeronautics and Space Administration's Johnson Space Center (NASA-JSC), per my specifications. A photo of the rack mounted cycler and its adjacent battery chamber is depicted in Figure A1. The cycler consist of 10 power supplies and 10 charger assembly racks. The cycler is designed to test rechargeable batteries and automated commercial charging circuits. During the charge state, the power supplies feed the chargers which charges the batteries. During the discharge state, the batteries are discharged directly through those same power bipolar supplies. The current limits of each of the 10 battery stations are 20 V and 10 A and are dictated by the bipolar power supplies used. The brain of the cycler is a Macintosh computer which talks to a power controller which switches batteries from state to state (charge, discharge, and off) and a Kepco Talker/Listener Device (TLD) to control the power supplies. The batteries are secured onto a holder which fits into a thermal chamber. Custom software routines were generated in LabVIEW to acquire the data, control the cycler based on this data, and decide whether to store the data. This appendix in details describes the design, specification, and operation of the cycler for the benefit of this thesis and any further users of the cycler.

Data Acquisition Units

The cycler has two Fluke Hydra Data Acquisition Units, P/N 2620A, each with 20 data channel scanning capability along with 8 digital output channels. Each unit is controlled via a RS-232 computer link. The pair allows for the acquisition of battery voltage, current, and temperature for 10 batteries. No external signal conditioning is necessary. Refer to the Hydra User Manual for more specifications. In the current configuration, one Hydra (Port 0) scans voltages and currents and puts out a 7 digital bit signal for relay switching to the Relay Controller. The other Hydra (Port 1) scans temperatures and puts out a single digital bit signal to the Watdog Timer in the Relay Controller.

Relay Controller

The Relay Controller was designed and built at NASA-JSC to contain all the relay drivers. It is located at the top of the rack. It uses the digital output signals from one Hydra and opens/closes charge and discharge relays for each battery station. The seven digital bit signal uses bits 0 through 3 to specify the station, bit 4 to specify charge or discharge, bit 5 to specify on or off, and bit 6 to enable and disable the signal. Bit 7 is displayed on the front panel but not used. The digital bit signal can be manually controlled from the front panel by flipping each bit in the manual position. The Relay Controller has individual light emitting diode (LED) indicators to indicate which charge and discharge relays are open/close. The Relay Controller also houses the Watchdog Timer which is a safety device to monitor the alertness of the computer. The timer will open all relays if the computer does not send it a simple digital signal at least once every 60 seconds. On the front panel, the timer can be turned on or bypassed. LED indicators show when the timer is receiving its periodic signal from the computer and whether it has timed out or not.

Charger Assembly Racks

The Charger Assembly Racks as shown in Fig. A2 were design and built at NASA-JSC and each contains a charger circuit board, charge and discharge relays, and a current shunt. These racks are designed to be slipped into any of the 10 stations. The front panel allows one to manually set the relays to charge or discharge and to set the charge rate to high or low. The LED indicators show what state the chargers are in. Each rack has a fuse located it back panel for overcurrent protection.

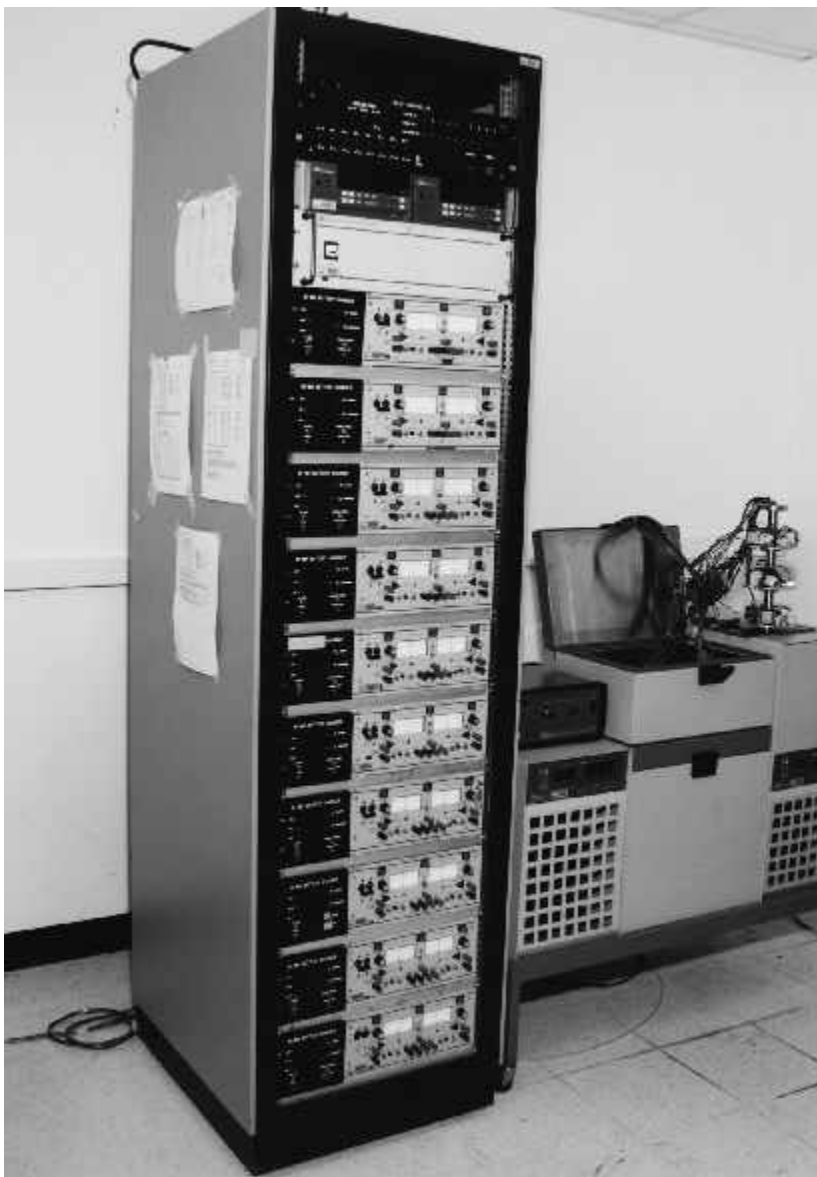


Fig. A1. Automated 10 Station Battery Cycler with adjacent calorimeter. Power supplies are adjacent to Charger Assembly Racks. Batteries are positioned in 3 layer holder placed on top of calorimeter.

GPIB Talker-Listener Device

The Kepco TLD 488 converts digital General Purpose Interface Bus (GPIB) signals from the computer to analog signals for communication with the power supplies. The TLD does this via A/D cards, TL-488-4B. Each can talk to four power supplies. The TLD contains three such cards. At the power supply end, an interface card, -PCA X-3 processes the analog signal.

Power Supplies

Each station has its dedicated Kepco BOP 20-10M power supply. This is a bipolar four quadrant supply capable of constant current or constant voltage control to 20 volts and 10 Amps. A green indicator light labeled "Remote" is on when the supply is under TLD control, otherwise it can be operated from its front panel. Refer to the Kepco BOP 20-10M Manual for details.

Computer

A Macintosh IIfx computer with 20 MBytes of Random Access Memory (RAM) and an 1 GByte harddisk is used to run the software controlling the Stand. It is equipped with two internal cards. One from National Instruments, NB-GPIB, for GPIB communications and the other from Applied Engineering, Quadralink, which provides four additional RS-232 ports. For data transfer, an ethernet link is available on the computer to link it to any other computer.

Software

The controlling, data acquisition, and data logging software is written as virtual instruments (VI) in LabVIEW® 2.2.1. The main VI is called "Battery Cycler." It controls battery cycling and performs the necessary data acquisition. The data recording is done by a VI called "Batt Hist." It stores all the channels of data into a binary format which is ideally suited from analysis using Igor. Battery Cycler and Batt Hist operated concurrently. The watchdog timer is supplied with its necessary pulses by the VI "Watchdog" which is a subVI to Battery Cycler.

Chargers

All charge methods were set at the same current, 2.3A. The simple galvanostatic charge method terminating when the battery reached 45°C, using a thermocouple placed on the battery, was achieved without any commercial charger circuit. The "smart" galvanostatic charge method was achieved with the Benchmarq bq2003 integrated circuit (IC) controller which terminated upon a seeing a negative voltage slope or reaching a certain positive temperature slope. The "burp" method was achieved with the ICS1702

controller from Galaxy Power, Inc. This chip provided the reverse pulse charge waveform shown in Figure 1 and terminated after seeing a voltage infection. The reverse pulse or discharge “burp” was achieved when with IC switched the battery to a resistor, sized to produce the desired discharge current. The “pause” method was achieved with the same IC controller except that the discharge pulse resistor was removed from the circuit. This resulted in a 29 ms OCV rest during every period of the waveform. One shortcoming with all these controllers is that they provide no means of detecting which of the multiple termination algorithms was responsible for terminating charge.

Battery

The Sanyo HR-4/3AU NiMH cell rated at 2400 mAh was used extensively for this work. Previously comparisons of competing commercial cells shown that at the time this design yielded the best C-rate capacity coupled with the most consistent cycling results. The batteries consisted of four cells in series which were mounted on a 3 layer cylindrical holder. The edge plates of the holder provided a conductive path to the walls of the cylindrical chamber of the calorimeter. These plates have many large holes to allow the necessary wire paths and allow air circulation through each level. One thermocouple and one thermistor were taped on each 4-cell battery.

Thermal Chamber

The batteries are maintained in isothermal environment by resting the 3 layer holder in the cylindrical chamber of the S77XX Heat Conduction Calorimeter, manufactured by Hart Scientific, Inc. The cylindrical chamber was immersed in a controlled water bath. Above the calorimeter chamber, an air circulation bath also help maintain at consistent thermal environment for the batteries during the cycling. The water and air baths of the calorimeter were set at 23°C temperature of the experiment described herein. Both baths have to capability to be set at any temperature between 0 and 80 °C.

Charger Installation

The chargers assembly racks were mounted into their respective rack slots (see Fig. A2.) after having its charging parameters set. Each is connected to by four quick-disconnects; one to a power supply, one to a battery with thermistor, one to a Hydra for current measurement, and the last to the relay controller. This allows one to easily remove and reinstall a charger for modifications. Whenever these charging trays are removed from the rack, one should verify that its fuse is still operational and replace as necessary.

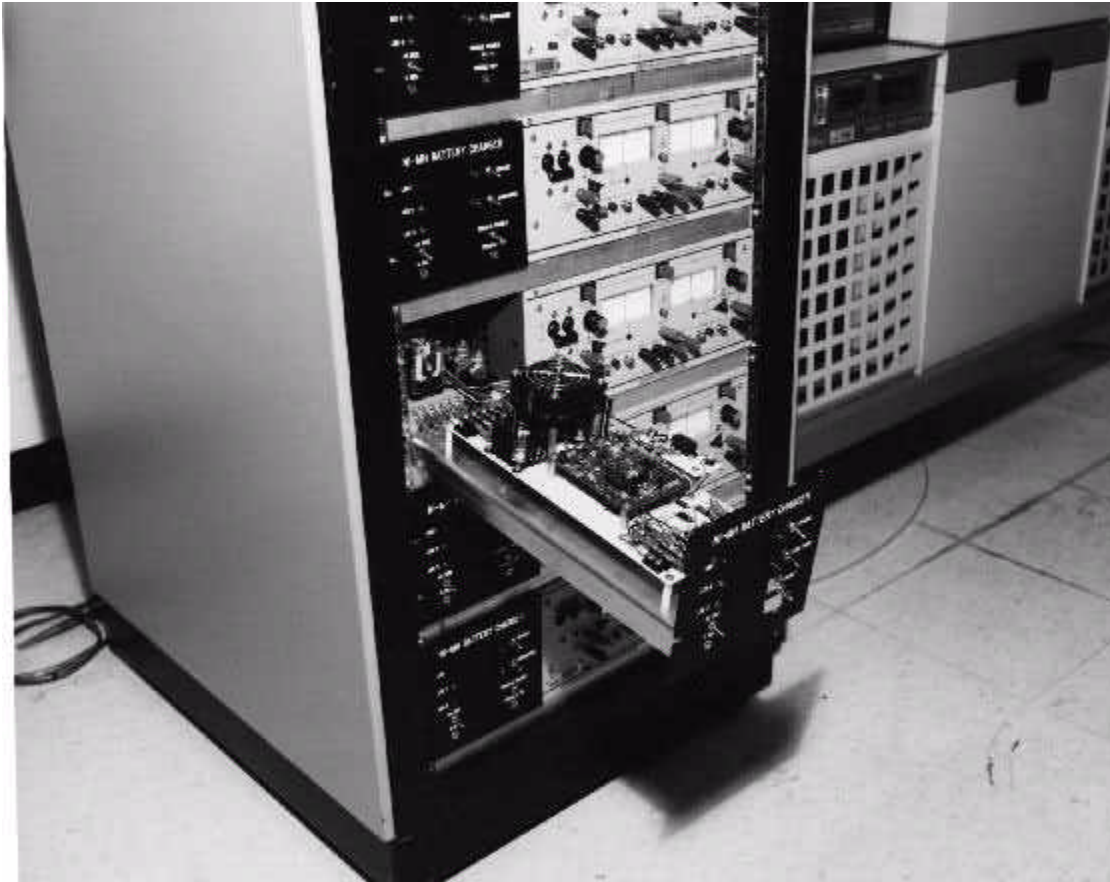


Fig. A2. Close-up of a charger assembly rack partially retreated from its slot to show its charger controller IC on printer circuit board in front of small fan.

Battery Installation

The batteries to be tested are secured into a designated slot on the three tier holder. Then, the appropriate power leads are soldered to each battery tab. Sense leads and thermistors must be tied directly to each battery. Leaving the air bath of the calorimeter, the thermistor leads and power leads are bundled together. Similarly, the sense leads and the thermocouple leads are bundled together leading to a break-out board behind the calorimeter. Once the voltage sense leads and thermocouple leads are connected, data

connections can be verified on the front panel of the Hydras. The Hydra on port 0 should be configured for channels 1 through 10 to read voltages. Channels 11 through 20 should be configured with a multiplicative factor of 100 to read currents in amperes. Channels 1 through 10 on the Hydra on port 1 should be configured for T type thermocouples. Once this was done, no further signal conditioning was needed.

Stand Start/Stop

Starting the battery cycling process should begin first by opening the data logging VI called "Batt Hist". Before executing it, a number of parameters must be set or verified on its front panel. Number of channels should be set to 40 to record ten state times, voltages, currents, and temperatures. Samples per channel set the length of each logging file. The first such file is labeled by the user and automatically suffixed with a "00". When the sample per channel limit is reached by any channel, subsequent data is logged into a new file with the suffix "01" and so on. A 3000 samples per channel setting will result in roughly a 1 MByte datafile. The "Save Every" parameter determines how often data is evaluated for storage. Fifteen is the fastest setting.

In the "Chan #" cluster array several parameters are set for each channel. The "Deadband" and "Fencepost" features tell HIST to log a channel value whenever that value is not within the deadband of the previous value or whenever the fencepost time has elapsed. Also in the cluster, each channel must be titled and given units. Refer to the HIST manual for more details.

The "Plot" option displays a real time plot of a selected channel from the beginning of the current file contents. This particular region of this plot can be expanded by defining appropriate beginning and end times. Turning off this plotting option relieves the computer to handle other tasks more efficiently.

Executing VI Batt Hist.

First, turn on each battery station which you want cycled. Select a discharge current in Amps (positive) and the number of cycles desired for each battery. The state of and the number of cycles completed by each battery are displayed. Next, set up the Battery Cycler VI by setting the parameters in Cluster titled "Key parameters of Battery Station". The duration of trickle charge and the rest periods after discharge and trickle charge are user selectable for each battery station. The Discharge phase of a battery is

terminated when its voltage dips below the user selected "discharge cut-off voltage". The Charge phase is nominally terminated by the charger's internal logic circuitry. However, if a battery voltage or temperature exceeds the user selected "charge voltage limit" or battery temperature limit, Battery Cycler will terminate the charge and switch on to Trickle Charge. The onset of the Trickle Charge phase of a battery is initiated once the battery current is detected to be lower than the user selected "trickle current threshold".

If one prefers to trickle charge at a selected constant rate rather than the rate set by the charger, then, setting the "Trickle w/ Kepco" switch to "yes" and setting the corresponding current in the "trickle charge current" array will do just that. If some of the charging assemblies require constant current input rather than constant voltage, these must be identified in the "charge input" switch. Constant current is denoted "CC" while constant voltage, the default setting, is "CV".

If one prefers to bypass the chargers in the tray and use the Kepco power supply directly, then, setting the charge time to zero will skip through the charge phase and go to trickle charge. Kepco trickle charge can be set to any current up to 20 A. The same voltage and temperature limits exist for this "trickle" phase as with the normal charge phase. One should be careful in properly defining the time limit for this "trickle charge" phase.

Finally, one can decide whether to set-up filenames for cycle logging station highlights and for a restart folder. A dialog box will prompt you for these filenames. "No" to the "set-up files?" will cause the previous files to be used. The filenames and any error messages are displayed on the front panel. Upon executing Battery Cycler, the connected batteries will be cycled. The state of charge of each can be seen on the front panel of Battery Cycler. All the batteries will start in the Charge Rest state and show a "-1" cycle count which is zeroed once Discharge begins. The data of each can be seen on the front panel of Batt Hist.

When a battery station is turned off either by the user or by the Battery Cycler VI, it can be restarted in two simple steps. First, turn on the particular station control of the Battery Cycler. Then, execute the Station Restart VI after having selected the appropriate restarting conditions of that VI. It is suggested to rename the cyclelog file if a new battery is substituted in the battery station.

Data Reduction

The detailed data from the stand is stored by Batt Hist in binary files and the cycle highlights of each battery station is stored by Battery Cyclor in individual text files. The binary files come in pairs suffixed ".data" and ".ptrs" which can readily be loaded by Igor, a graphical data analysis software. Igor uses an XOP macro called "LoadHIST Channel" to do this. Refer to the Igor User Manual for more details and instructions. The final values of state time, voltage, current, and temperature of each battery state (discharge, discharge rest, charge, trickle charge, and charge rest) is recorded along with its cycle number and charge termination reason into a cyclelog file for each battery station. The user is prompted to name that file upon execution of Battery Cyclor. The values for each cycle are continually appended to the cyclelog file along with a time and date stamp as they occur.

Battery Cyclor VI Operation

The Battery Cyclor VI is composed of a two step sequence consisting of initializing instruments and files followed by a While Loop containing the main activities of Battery Cyclor. This While Loop is perform until all battery stations are turned off either by the user or by the program. The While Loop has a three step sequence which consists of (1) triggering a scan of all data channels and updating global variables and displays, (2) performing the main For Loop that evaluates what to do with the data, and (3) displaying key parameters and triggering the watchdog timer.

The main For Loop steps through each battery station and extract that channel's time stamp, voltage, current, and temperature from the latest scanned data, filters it for glitches, and loads it into a global variable called "Final Data". This same global variable is used in many other VIs and demonstrates one of the most powerful features of LabVIEW for passing information from one process to another. Global variables as 10 element arrays are used extensively in all VIs for the stand. For example, "Battery Station On/Off" keeps track of which stations are on. If a station is off, the main For Loop only updates the "Time Zero" global array and uses the "Power Controller" VI to open all that channel's relays. If the station is on, then if there is not a glitch in the data (values out of range), the "Cycle State" VI is called to decide if the battery should continue in that state, be switched to the following state, or turned off.

Cycle State is the most complex of the subVIs in Battery Cyclor because it uses the most input parameters. It uses the data from the global variable array "Final Data" and compares it to defined control parameters for deciding whether to call upon "New State" to switch state. The "Discharge" state is terminated only when the battery voltage dips below the discharge cut-off voltage control parameter. The following "Discharge Rest" state is terminated when the state time exceeds the discharge rest time control array parameter and when the battery temperature is below the temperature limit control parameter. The following "Charge" state is terminated when either of the following occurs; (1) charge current is below a trickle threshold control parameter which indicates trickle charging is occurring, (2) battery voltage exceeds battery voltage limit control parameter, or (3) battery temperature exceeds the control parameter limit. The following "Trickle Charge" state is terminated when either of the following occurs; (1) state time exceeds trickle charge time control array parameter, (2) battery voltage exceeds battery voltage limit control parameter, or (3) battery temperature exceeds the control parameter limit. The following "Charge Rest" state is terminated when the state time exceeds the charge rest time control array parameter and when the battery temperature is below the temperature limit control parameter. Upon termination of charge rest, the cycle count for that battery is incremented and compared to the cycles required control array parameter. If cycles completed exceeds cycles required, then Power Controller is called to turn off that station. If not, then New State is called. In both cases, the cycle highlights stored in a global variable array called "Cycle Endpoints" are stored to a file by the VI "Cycle Log".

New State uses the Power Controller VI to switch relays from on state to the following state. For every state switch, Power Controller is called to turn off the current state followed by turning on the new state. A couple complexities merit mention. Nominally, the chargers require an input of constant 11 volts. Certain chargers require a constant current input which is accomplished by telling the Power Controller to "discharge" the battery with a charging current through the discharge loop. The discharge relay indicators will be on but the battery will be charging. This simplifies the software and serves as reminder that this charger operates with a constant current input. User controlled constant rate trickle charging is also handled the same way though the discharge loop.

Batt Hist VI Operation

The VI "HIST" was purchased from Gary W. Johnson, Inc., in Livermore, CA, and modified into "Batt Hist" to fit the stand's purposes. The major modifications include using the global variable "Final Data" as the source of data and logging data into sequentially suffixed files. The 40 channel data of Final Data is put into format compatible with HIST by the VI "Final Data 1D"

Watchdog

The Watchdog VI simply tells one of the Hydra Data Acquisition Units to periodically send a digital I/O pulse to the Watchdog Timer circuitry in the Relay controller. If the VI fails to do so within a 300 seconds span, the timer will trip open all relays and not accept any new commands without being reset.

Restart Station

The VI "Station Restart" allows one to begin or resume cycling a battery after it has been turned off. One selects the station index to restart, what state it should start in, and what filename should log the highlights of its cycling. Prior to executing Station Restart, make sure that the boolean station on/off control on the front panel of "Battery Cycler is on. The key feature here is that Battery Cycler never has to be interrupted during this process. Therefore, the cycling of the other batteries is uninterrupted while making modifications to one or more batteries.

REFERENCES

"Ni-MH Battery Test Stand Schematic Drawings" by S. Hossain and B. Hughes, LMES, Jan 94.

Hydra, 2625A Data Logger and 2620A Data Acquisition Unit, Users Manual, Fluke, Inc.

Interactive Digital Programmer, Model TLD-488-16, Operator's Manual, Kepco, Inc.

Bipolar Operational Power Supplies Model 20-10M Instruction Manual, Kepco, Inc.

Benchmarq Charger Evaluation Board, product literature, Benchmarq, Inc.

Integrated Circuits Systems 1702 QuickSaver Evaluation Board,

User Guide to the S77XX Heat Conduction Calorimeter, TTA-OP-O-54

LabVIEW 2 User Manual, National Instruments, Inc.

HIST, Historical Trending Package for LabVIEW, User's Manual, Gary W. Johnson, Inc.

APPENDIX B

Design, Specifications, and Operation of the Cell Calorimetry Experiment

A heat conduction calorimeter, model # 5023, and custom 4/3A cell holder from Hart Scientific were used in this experiment as shown in Figure B1. The cylindrical calorimeter chamber is capable of accommodating cells as large as DD size. To provide proper heat conduction using a 4/3A cell, the cell is stripped of its insulating sleeve and inserted into the holder. The fit is very snug to maximize thermal contact. Heat from the cell is conducted to the cylindrical wall of the calorimeter chamber which contains thermoelectric sensors.

The calorimeter operates on the Seebeck or thermocouple effect. As heat is conducted through the thermoelectric device, a voltage is produced which is proportional to the temperature difference across the thermoelectric device. The water side of the thermoelectric sensor is maintained a constant temperature by virtue of the continuously-circulating, temperature-controlled water bath. As the temperature of the test article side of the thermoelectric sensors fluctuates, the proportional voltage signal recorded is a measure of the heat flow through the sensors.

The water bath maintains the water temperature within ± 0.01 °C. The sensitivity of the heat measurement is 100 μ W. The measurements are calibrated by replacing the cell in the holder with a resistor simulating the heat generation levels of the cell. With precise knowledge of the electrical power input into the calibrating resistor, a calibration factor is obtained for the experimental conditions that converts the voltage reading of the thermoelectric sensors into a heat value. By calibrating with similar current levels and external heat disturbances, most sources of error are canceled out. Accuracy of the calibration measurement was within ± 0.5 mW.

For this experiment, one of the 4 cells from the battery packs which were cycled 400 times was placed in the holder. The other 3 cells were placed on the outside top of the calorimeter and connected in series to the cell inside the calorimeter. Together electrically, the 4 cell pack was cycled 25 times with one of the stations of the cycler described in Appendix A. Voltage sense leads connected very close to the cell tabs inside the

cell holder were provided for an accurate voltage measurement. The sense and power leads were built into the holder stand-offs.

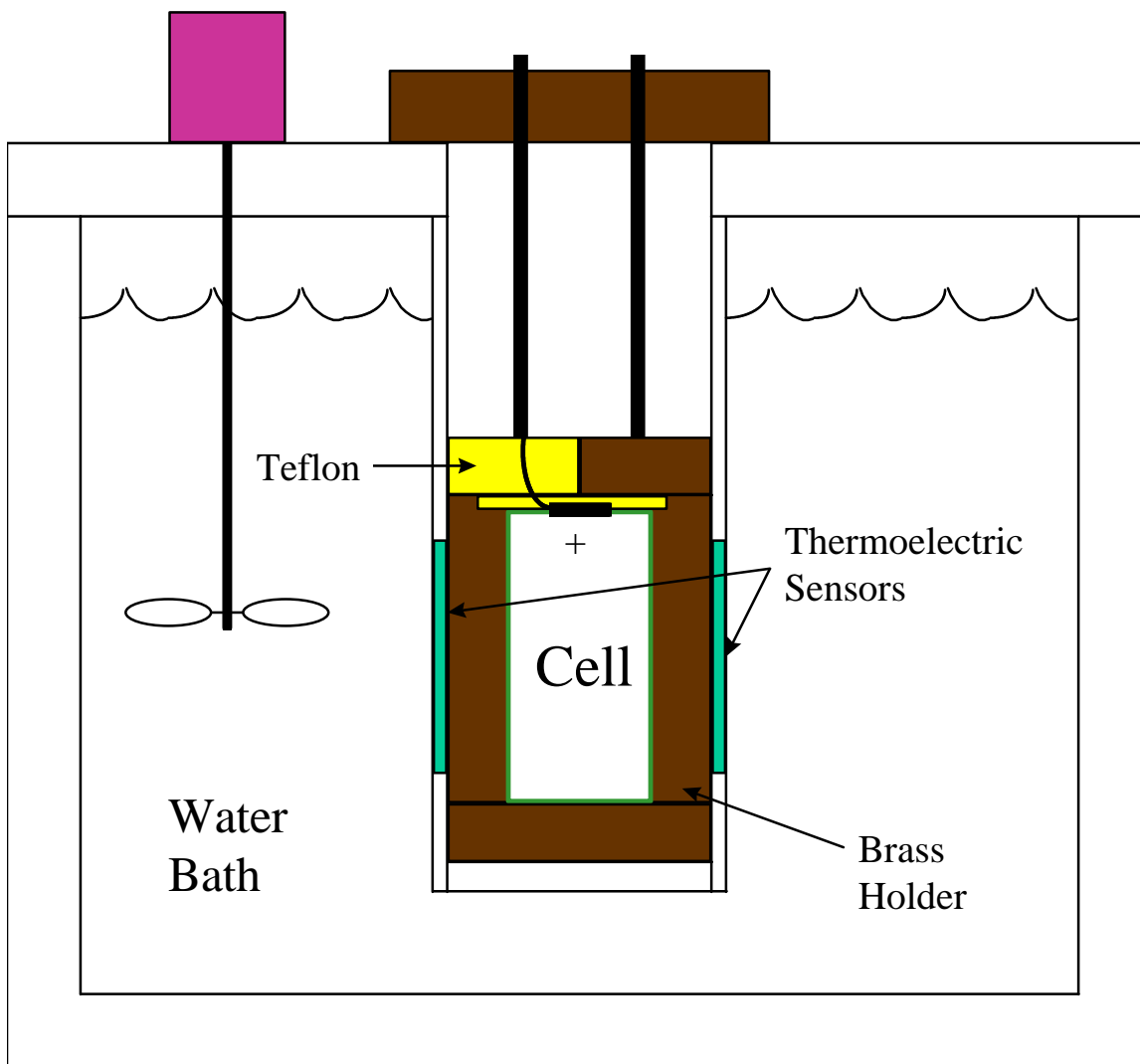


Fig. B1. Cross section of cell calorimetry experiment.

APPENDIX C

Set-Up and Procedure for Destructive Physical Analysis (DPA)

Disassembly

All cells were disassembled in a fully charged state inside an argon filled glove box, manufactured by Vacuum/Atmospheres Company. Prior to each cell disassembly, the glove box was purged with argon until a purity of >99% was confirmed by gas sample analysis by gas chromatography. Humidity of the glove box was maintained between 20% and 40% and measured by a hygrometer to prevent cells from drying out during disassembly. The purpose of the inert environment was to prevent oxidation of active material and due to the pyrophoric nature of some metal hydrides.

While inside the glove box, cells were stripped of their insulation and tabs. A miniature lathe manufactured by Sherline (P/N 60428) was used to make a circumferential cut just below the crimp seal of the cell. The positive tab was cut to separate the top of the cell from the rest of the cell assembly. The sharp metal cutters, a small cut in the can was made next to where the outer electrode ends two layers of separator overlap each other. With needle-nose pliers, the cell can was peeled away until electrode coil was released. The negative tab, which consists of a metal ring which is welded to the edges of the negative current collector, was peeled away to free the electrode coil. At this point, the separator overlap which is glued to the inner separator layer is maintaining coil compression. Using a sharp blade, the separator glue joint was undone which permitted uncoiling the jelly-roll electrode coil. The cell's dual separator design meant that each electrode was wrapped in separator.

Once each electrode and separator were separated, each was rinsed three times in de-ionized water to remove as much KOH deposits as possible. After a one hour drying time, coupons of each electrode and separator were obtained, double bagged, and removed from the glove box.

The coupons for the SEM and EDS analyses were prepared by cutting 1 cm square coupon of each electrode material with its current collector. I designed a custom coupon holder to keep the coupon sealed from the ambient environment until a vacuum had been achieved. Then, a gear mechanisms on the holder allowed it to be remotely opened for viewing by the SEM. Special attention was paid to not disturb the

surface of the specimen coupons. For the surface area and pore size distribution analysis of the positive electrodes and the particle size analysis of the negative electrodes, specimens were obtained by gently scrapping the active material off their respective current collectors.

For the surface area and pore size analysis was performed with a Coulter SA 3100 surface area and pore size analyzer manufactured by Coulter Corporation. All specimens were out-gassed at 70 °C for 60 minutes prior to measuring the BET surface area using helium.

For the particle size analysis of the negative hydride, all specimens were prepared in a test tube to with 2 ml of water with a drop de-agglomerizer added. The specimen solutions with the insoluble active material were treated to the same 2 minute ultrasonic treatment. The analysis was performed with a Horiba LA-910 laser scattering particle size distribution analyzer manufactured by Horiba Instruments Inc. Each specimen was further agitated for 5 minutes and circulated for 7 minutes in the instrument prior to the measurement.

APPENDIX D

Set-up and Procedure for Video-Microscopy

For the in-situ video-microscope experiment, the cell coil was uncoil only enough to allow a small 1 cm square corner cut of the outer hydride electrode and the adjacent separator layers to expose the positive nickel electrode. The coil compression was regain with tie-wraps as shown in Fig. D1. The coil was double bagged and removed from the glove box.

Sturdy nickel strips 1 mm thick were spot welded to the tabs of the coil. The strips were fed through to a customized rubber stopper made for a 1 L polymethylpentene beaker. The beaker material was chosen for its tolerance to KOH attack and for its transparency. A 6.4 M solution of KOH was prepared and sparged for 2 hours with nitrogen gas to remove dissolved oxygen to prevent formation of carbonates. After the solution was pour into the beaker to a level that immersed the exposed nickel electrode window of the coil, the head space of the beaker was purged with nitrogen gas and sealed. All the above steps were performed in one day to preclude long exposure of the cell and electrolyte to the ambient environment.

A video microscope system consisted of a video-microscope, Model PV10 CB, with a 10 to 70X magnification lens, Model OVM-70X, and a high intensity light source, Model PV10-PS, all manufactured by Olympus Corp. The lens was secured in place with a stand adjacent to the outside of the beaker wall directly facing the area of interest of the electrode coil. The video output of the video-microscope was fed to a VCR/TV system.

The desired current waveform was achieved by programming a Macintosh computer equipped with a analog output card. This voltage signal was amplified by the Preston amplifier and fed to the current control input of a bipolar power supply/amplifier, Model BOP-20-10M, manufactured by Kepco Instruments, Inc. With the power supply in the current control mode, the voltage signal input into the power supply produced the desired current waveform. This waveform was verified to be accurate within ± 1 mA with a calibrated digital oscilloscope. Voltage and current data were measured and acquired with a Hydra Data Acquisition Unit from Fluke, P/N 2620A. A LabVIEW VI was generated to control waveform and record the voltage, current, and time data.

An audio signal was provided to the VCR to signal the occurrence of discharge pulse or relaxation pause in the charge waveform. This signal was short beep made possible by connecting a buzzer to a voltage comparator which triggered the beep every time the voltage signal from the computer was \leq zero volts. This beep was amplified by microphone and the resulting audio signal was fed to the VCR audio input.

The cell was discharged by connecting it to a 0.5 ohm resistor to 1.0V. After waiting 5 minutes, a residual discharge at 1 ohm to 1.0V followed. The cell was allowed to rest > 15 minutes prior to the charge cycle according to the current waveforms described in Table 1. The nearly C-rate charge was terminated after < 70 minutes or earlier depending on the vigorous nature of the bubbling activity.

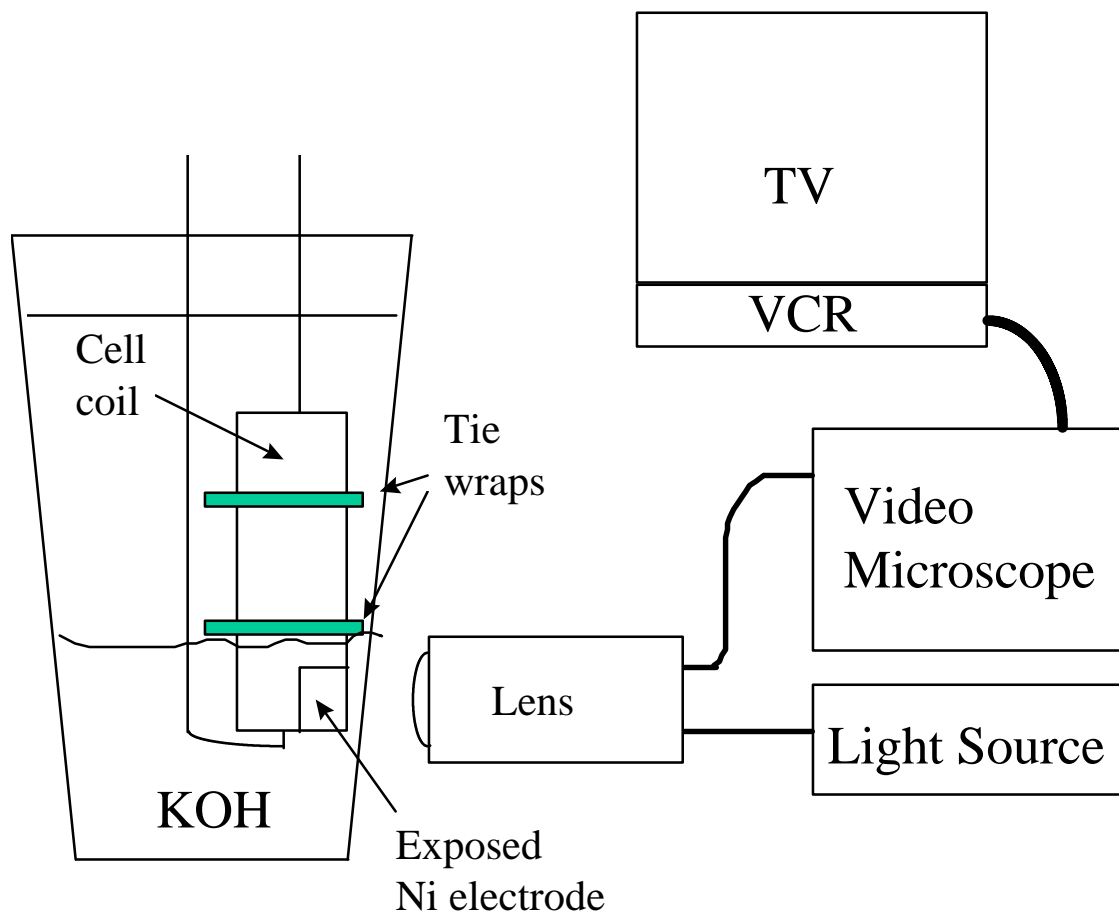


Fig. D1. Schematic of the in-situ video-microscopic experiment. Charge/discharge cyclers and electrical connections not shown for clarity.

APPENDIX E

Set-up and Procedure for Manometry

For the manometric experiments, complete fresh cells were used that were equipped with solderable tabs. The cells were cycled at room temperature at C/2 rate 10 times to ensure their capacity performance was nominal. A very small hole was drilled into the middle of the negative end of the first cell. The cell tabs were soldered to wires which were soldered to nickel strips fed through a rubber stopper. The cell/stopper assembly was sealed in a graduated cylinder filled with glass spheres used to consume volume. The polypropylene tubing network connected the cell to a manometric gauge, Model E-00905, from Cole-Parmer Instrument Co. The gauge is designed to be used with 15 ml of mercury and has a readable level range of 20 cm. De-ionized water was used instead to provide more pressure sensitivity.

The manometer was calibrated by introducing known volumes of nitrogen gas with a syringe through the rubber stopper. For example, insertion of 1 ml of gas, produced a 4.1 cm displacement in the manometric reading.

The cycling control of the cell was performed with same set-up as in the video-microscopic experiment. Charger was terminated when cell voltage reached 1.550V. Voltage sense leads were connected to the nickel strips outside the rubber stopper. This introduced an extra 11.6 mohm of resistance that would have been avoided if the sense lead could have been on the cell terminals. In comparison to the test cell for the calorimetric experiment, the analogous resistance was measured at 4.5 mohm. This explains why the overvoltage of the manometric experiments were about 10 mV higher while running at 2.0 A than the overvoltage of the calorimetric experiments running at 2.3A.

The set-up for the flooded cell experiment varied slightly. A small hole was drilled into the centers of both ends of the cells. The cell positive was placed on top to allow flooding the cell with 6.4 M KOH without immersing the positive lid of the cell. The KOH solution was prepared as in appendix D. The head space of the cell and manometer were purged with nitrogen before the cell rested for > 1 week to ensure complete flooding. More electrolyte was introduced and a subsequent purge followed to the first charge/discharge cycle. Cell was allowed to rest for 2 more days, before the experiment started. For every charge method, two charge/discharge cycles were performed and the second cycle was used for comparison. This prevented variations due to various lengths of storage stand time. The rest time between the first and

second cycle was kept consistent at one hour and was not enough time to have cell pressures return to the starting ambient pressure. Therefore, cell pressure was equalized to ambient pressure before the start of the second charge/discharge cycle to re-zero the manometer.

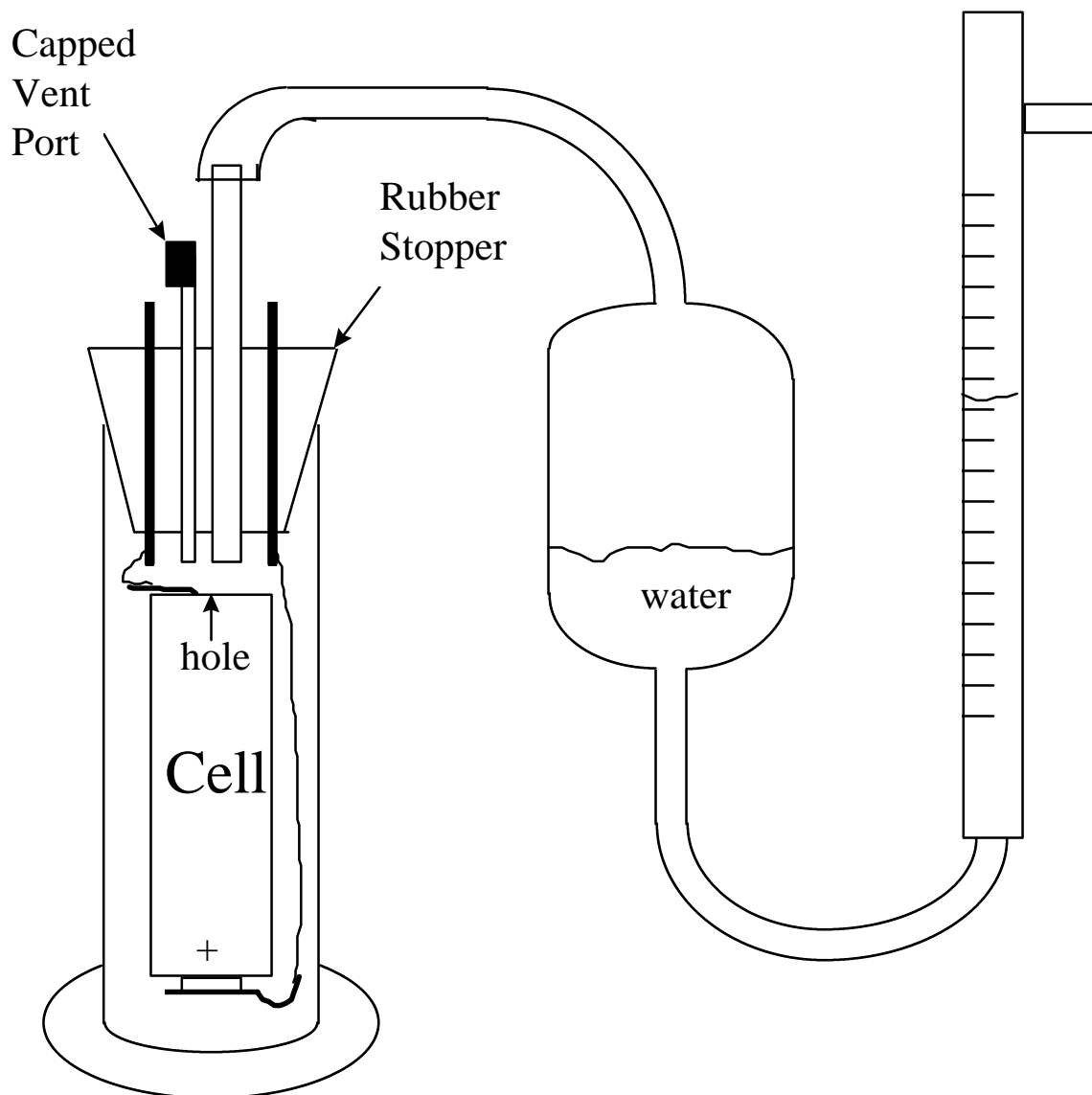


Fig. E1. Configuration of nominal cell with manometer. Glass spheres taking up extra volume in cylinder containing cell are not shown for clarity. Cell had small hole drilled into its negative end.

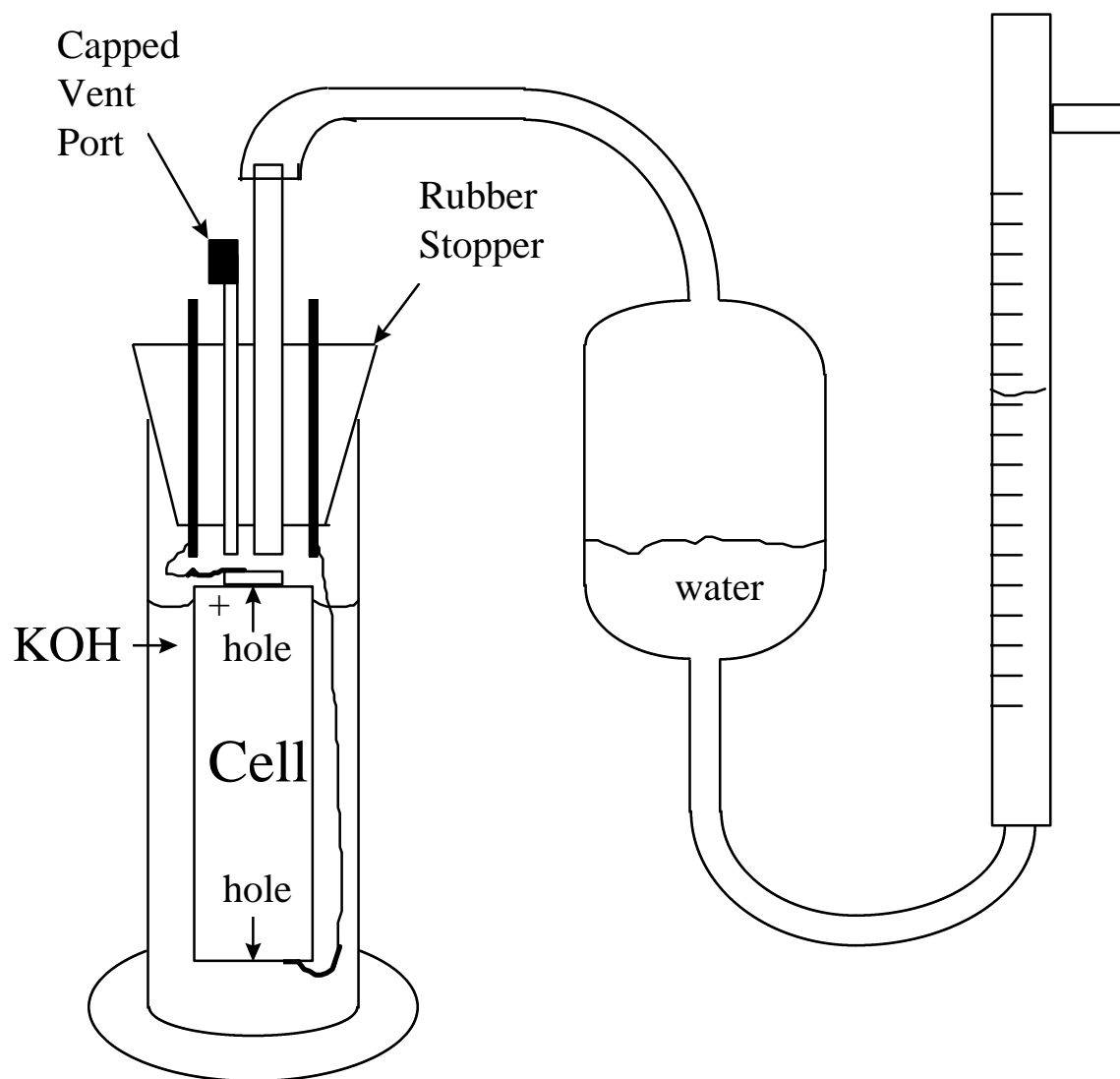


Fig. E2. Configuration of flooded cell with manometer. Cell had small holes drilled into its negative and positive ends.